E-ISSN: 3023-784X

Advanced Radiology and Imaging

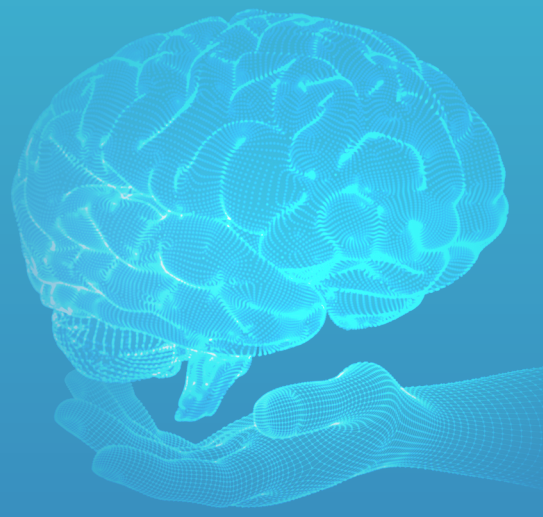

VOLUME 2 / ISSUE 1

APRIL
2025

galenos Publishing House

ARI

advradiology.org

advradiology.org

Advanced Radiology and Imaging

VOLUME 2 / ISSUE 1
APRIL 2025

EDITORIAL BOARD

VOLUME 2 / ISSUE 1
APRIL
2025

Advanced Radiology and Imaging

advradiology.org

Please refer to the journal's webpage (**https://advradiology.org/**) for "**Journal Policy**" and "**Instructions to Authors**".

The editorial and publication process of the Advanced Radiology and Imaging are shaped in accordance with the guidelines of the **ICMJE, WAME, CSE, COPE, EASE,** and **NISO**. The journal is in conformity with the Principles of Transparency and Best Practice in Scholarly Publishing.

Advanced Radiology and Imaging is indexed in **Türkiye Citation Index, IdealOnline, Zenodo, Scilit,** and **Index of Academic Documents.**

The journal is published online.

Owner: Galenos Publishing House

Responsible Manager: Sonay Aydın

Publisher Contact
Address: Molla Gürani Mah. Kaçamak Sk. No: 21/1 34093 İstanbul, Türkiye
Phone: +90 (530) 177 30 97 / +90 (539) 307 32 03
E-mail: info@galenos.com.tr/yayin@galenos.com.tr
Web: www.galenos.com.tr
Publisher Certificate Number: 14521

Publication Date: April 2025
E-ISSN: 3023-784X
International scientific journal published quarterly.

advradiology.org

Advanced Radiology and Imaging

VOLUME 2 / ISSUE 1
APRIL 2025

CONTENTS

Research Articles

Case Report

RESEARCH ARTICLE

DOI: 10.4274/AdvRadiolImaging.galenos.2024.55265
Adv Radiol Imaging 2025;2(1):1-4

Sacroiliac Joint Variants: Insights from a Retrospective Computed Tomography Study

Emre Utkan Büyükceran[1], Sezer Kula[1], Kemal Buğra Memiş[2]

[1]*Iğdır State Hospital, Clinic of Radiology, Iğdır, Türkiye*
[2]*Ankara University Faculty of Medicine, Department of Radiology, Ankara, Türkiye*

Abstract

Objective: This study aimed to determine the prevalence and distribution of sacroiliac joint (SIJ) variants based on age and sex using computed tomography (CT) and to investigate their clinical relevance.

Methods: This retrospective study analyzed pelvic and abdominal CT scans from 200 patients aged 18 years and older, focusing on SIJ variants. Variants were evaluated by two radiologists, and their associations with age and gender were assessed.

Results: SIJ variants were observed in 107 patients (53.5%), with a mean age of 38.65±22.29 years. The most common variant was the iliosacral complex (44.9%), followed by the accessory SIJ (27.1%). A significant association was identified between variant types and age groups (p=0.005), whereas no significant relationship was found with gender.

Conclusion: SIJ variants are prevalent and exhibit age-related differences. Awareness of these variants is essential to avoid misdiagnosis and ensure proper clinical management.

Keywords: Sacroiliac joint variants, ileosacral complex, accessory sacroiliac joint, computed tomography, prevalence, age-related variants

Introduction

The sacroiliac joints (SIJs) are the largest axial joints in the human body and connect the axial skeleton to the pelvis. Due to their complex anatomical structure, they are one of the most challenging joints to assess using radiological imaging.[1,2]

With the widespread use of magnetic resonance imaging and particularly computed tomography (CT), significant advancements have been made in the diagnosis of SIJ disorders.[3] Understanding the normal anatomical structure of SIJs is essential for accurately identifying pathologies. SIJs exhibit a wide range of structural variations and may undergo certain anatomical changes.[4] Therefore, comprehensive radiological studies play a crucial role in distinguishing between normal and pathological appearances, providing significant benefits in the diagnosis of SIJs disorders.

Knowledge of the radiological morphology of the SIJ is crucial for the evaluation of spondyloarthropathic, such as ankylosing spondylitis, as well as degenerative conditions like osteoarthritis and processes arising from mechanical overloading. Additionally, this understanding is essential in surgical procedures, such as posterior pelvic fixation and both closed and open reductions.[5-8]

Numerous studies have identified the presence of an accessory sacroiliac joint (ASIJ) as the most common anatomical variant. The majority of these studies were conducted through direct observation of anatomical specimens.[9] A potential correlation between the presence of SIJ variations and factors such as sex and age has been suggested.[9] More recent studies have reported the normal anatomy of the SIJ using CT, direct radiography,[4] and cadaver specimens.[2,10]

Prassopoulos et al.[11], proposed a classification of six anatomical variants, reporting a prevalence of 36.3% in the Greek population. Demir et al.[3], reported a higher prevalence of 41.8% in the Turkish population.

However, debates regarding the origin of these variants persist; it remains unclear whether they are congenital or acquired later in life.[12] This study aimed to determine the types and prevalence of SIJ anatomical variants using Prassopoulos' classification via CT while also examining their associations with sex and age.

Cite this article as: Büyükceran EU, Kula S, Memiş KB. Sacroiliac joint variants: insights from a retrospective computed tomography study. Adv Radiol Imaging. 2025;2(1):1-4

Address for Correspondence: Emre Utkan Büyükceran MD, Iğdır State Hospital, Clinic of Radiology, Iğdır, Türkiye
E-mail: utkan.buyukceran91@gmail.com **ORCID ID:** orcid.org/0000-0001-6912-7737
Received: 24.10.2024 **Accepted:** 25.11.2024 **Epub:** 27.11.2024 **Published:** 30.04.2025

Methods

This study was approved by the Non-interventional Clinical Research Ethics Committee of Erzincan Binali Yıldırım University (decision no: 2024-12/03, date: 12.09.2024). Informed consent was obtained from all patients prior to undergoing CT scans. Since the study was conducted retrospectively, no additional informed consent was required beyond what was initially obtained.

This retrospective, observational, cross-sectional, and descriptive study included consecutive pelvic and full abdominal CT scans performed at the Radiology Clinic of Iğdır State Hospital. All scans were acquired using a Siemens Emotion 16-slice CT scanner (Siemens Healthcare, Erlangen, Germany, 2007).

The sample size calculation was based on an expected moderate effect size of 0.5, significance level of 0.05, and power of 0.8. The inclusion of 200 patients was sufficient to detect statistically significant differences in SIJ variation.

Between 1 June 2024 and 1 July 2024, all CT scans performed at our hospital were reviewed in chronological order. The screening process was terminated after 200 patients met the inclusion and exclusion criteria.

The inclusion criteria were CT scans of patients older than 18 years with the SIJ fully visible. The indications for CT scan included acute abdominal pain and suspected intra-abdominal or pelvic pathologies, such as gastrointestinal, urological, or gynecological diseases. The exclusion criteria included conditions that could complicate the evaluation of variations, such as multiple traumas, spinal surgeries, and injuries.

Each CT scan was evaluated by two radiologists to determine the presence of anatomical variations. Assessments were conducted using bone-window view of the CT scans, focusing on the classification of variants. The evaluations were not blinded, and a consensus between the two radiologists was reached regarding the presence and type of variation, if any.

Statistical Analysis

All statistical analyses were performed using Statistical Package for the Social Sciences version 23 (IBM, Armonk, NY, USA). Descriptive statistics were reported as mean±standard deviation for normally distributed numerical variables and as median (minimum-maximum) for non-normally distributed data. Categorical variables are presented as numbers and percentages. Comparisons between groups with normally distributed data were made using the Student's t-test, while the Mann-Whitney U test was used for non-normally distributed data. The chi-square test was used to analyze categorical variables. A p value ≤0.05 was considered statistically significant.

Results

Between June 1, 2024 and July 1, 2024, CT scans were systematically reviewed in chronological order of acquisition, and a total of 200 patients were included in the screening process. Sacroiliac variants were detected in 107 patients (53.5%). Representative CT images of SIJ variants are shown in Figure 1.

The mean age of patients with sacroiliac variants was 38.65±22.29 years, ranging from 18 to 91 years. Of the 107 patients, 82 were male (76.6%) and 25 were female (23.4%). The distribution of patients by age showed that 40 patients (37.4%) were over 40 years old, while 67 patients (62.6%) were under 40 years old. The variants were primarily bilateral in 62 patients (57.9%), with 21 patients (19.6%) having variants on the right side and 4 patients (3.7%) on the left side.

Regarding the specific sacroiliac variants, the ileosacral complex was the most common, observed in 48 patients (44.9%), followed by the ASIJ in 29 patients (27.1%). The crescent iliac bony plate was identified in 15 patients (14.0%), ossification centers in 7 patients (6.5%), and both bipartite iliac bony plate and semicircular defect in 4 patients (3.7%) each. The distribution of SIJ variant types, demonstrating the predominance of the iliosacral complex as the most common variant, followed by the ASIJ, is illustrated in Figure 2 and summarized in Table 1.

The analysis revealed no significant relationship between gender and variant types (p=0.083). However, age and variant types showed a statistically significant relationship (p=0.005). Patients under 40 years old most commonly had the ileosacral complex (35 patients) and ossification centers (7 patients), whereas patients over 40 predominantly exhibited the ASIJ (18 patients). This relationship is visually demonstrated in Figure 3, in which age-based differences in variant types are clearly observed.

Discussion

This study revealed a high prevalence of SIJ variants (53.5%), which was within the upper range of previously reported values in the literature

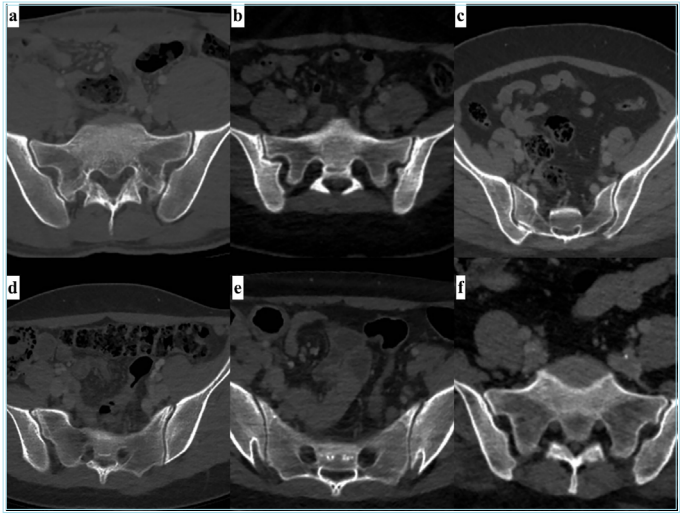

Figure 1. Representative computed tomography images of sacroiliac joint variants. (a) Accessory sacroiliac joint, (b) ileosacral complex, (c) crescent iliac bony plate, (d) ossification centers, (e) bipartite iliac bony plate, and (f) semicircular defect

Table 1. Distribution of sacroiliac joint variants

Sacroiliac variant	Number of patients (%)
Iliosacral complex	48 (44.9)
Accessory sacroiliac joint	29 (27.1)
Crescent iliac bone plate	15 (14.0)
Ossification centers	7 (6.5)
Semicircular defect	4 (3.7)
Bipartite intestinal bone plate	4 (3.7)

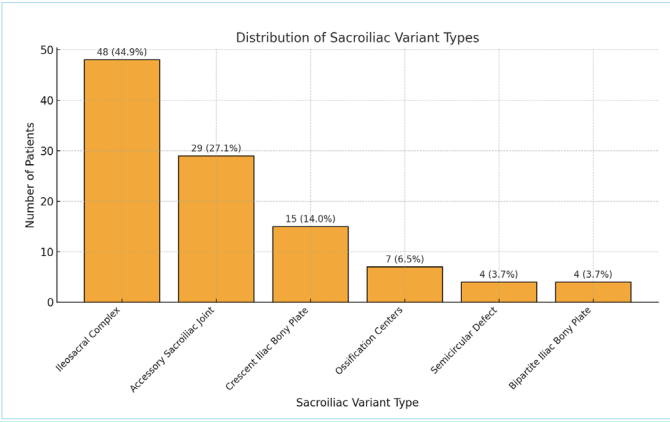

Figure 2. Distribution of sacroiliac variant types

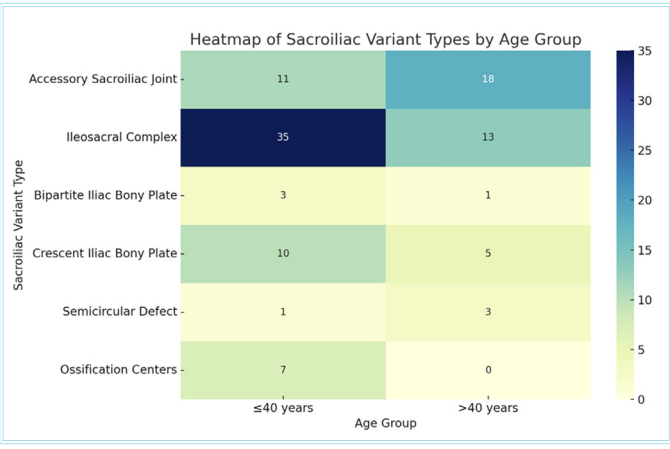

Figure 3. Heatmap of sacroiliac variant types according to age

(25.7-54.2%).[13] The most notable finding was the predominance of the iliosacral complex, particularly in younger patients, whereas the ASIJ was more frequently observed in older individuals. These findings suggest that SIJ variants may follow an age-related pattern, possibly influenced by cumulative mechanical stress or developmental changes. This highlights the importance of considering other factors, such as occupational- or lifestyle-related mechanical loads, as potential contributors to variant development.

The most common variant was the iliosacral complex 48 patients (44.9%), followed by the ASIJ 29 patients (27.1%). Similarly, Tok Umay and Korkmaz,[4] in their study involving 430 patients, also identified the iliosacral complex as the most prevalent variant. However, in many other studies, the ASIJ was reported as the most common variant.[3,9,11,14,15] The ASIJ is an additional joint within the ligamentous compartment, where the joint facets are covered by hyaline cartilage or fibrocartilage. The prevalence of this joint in individuals without SIJ disorders ranges from 4.5% to 26%.[3,4,9,11,14-18] This variant was observed to occur with equal frequency in both genders. Some studies have indicated that its prevalence increases with age and is more common in obese individuals and women who have had three or more childbirths.[3,9,11,17] In a study utilizing anatomical specimens, Trotter reported that accessory sacroiliac facets were more common among African women, attributing this to the cultural practice of carrying children on their backs wrapped in blankets.[19] In our study, the ASIJ was the most common variant in patients aged >40 years. This finding supports the hypothesis that ASIJ is not congenital but rather acquired over time due to factors such as mechanical stress.[20,21] In the younger population, the most common variant was the iliosacral complex. The ossification center variant, which is consistent with the literature, was not observed in the population over 40 years of age.[15]

No significant association was observed between gender and the variants in this study. Some previous studies have suggested that variants are more common in women.[9,3,18] Our results did not corroborate this finding.

It has been suggested that SIJ variants may be associated with past occupations or recreational activities, providing evidence for the theory of joint overuse. The fact that most variants were bilateral further supports the argument that mechanical stress may play a role in their development.[22] Changes caused by mechanical stress can result in radiographic images that mimic rheumatic diseases.[9,23]

Interpretation of the SIJ requires expertise. Although conditions such as low back pain and rheumatic diseases are primarily assessed using clinical criteria, imaging techniques play a crucial role in diagnosis, staging, and treatment monitoring. Anatomical variations can easily be mistaken for pathological findings, and accurate identification of these variants is essential for ensuring patient safety during surgical procedures. Due to the complex anatomy of the SIJ and the frequent occurrence of anatomical variants, misinterpretation of these findings is common.[20,24,25] Therefore, understanding normal variations is crucial for preventing the misinterpretation of pathological findings.[13]

Study Limitations

This study has several limitations. First, this was a retrospective study based on CT scans obtained from a single center, which may limit the generalizability of the findings to broader populations. Second, the sample size may not capture the full variability of SIJ anatomical variations across different ethnic and demographic groups. Additionally, the study did not include a follow-up period to assess the clinical implications of the detected variations, limiting the ability to evaluate long-term effects. Lastly, the lack of blinding in the radiological assessments could introduce potential bias, although a consensus between two experienced radiologists was reached for all cases.

Conclusion

This study highlighted the high prevalence of SIJ variants, particularly the iliosacral complex in younger patients and the accessory SIJ in older individuals. The significant occurrence of these variants underscores the importance of awareness in clinical practice to avoid misinterpretation during diagnosis and treatment.

Ethics

Ethics Committee Approval: This study was approved by the Non-interventional Clinical Research Ethics Committee of Erzincan Binali Yıldırım University (decision no: 2024-12/03, date: 12.09.2024).

Informed Consent: Informed consent was obtained from all patients.

Footnotes

Authorship Contributions

Surgical and Medical Practices: E.U.B., S.K., Concept: E.U.B., K.B.M., Design: E.U.B., K.B.M., Data Collection or Processing: E.U.B., K.B.M., Analysis or Interpretation: E.U.B., Literature Search: E.U.B., S.K., Writing: E.U.B.

Conflict of Interest: No conflict of interest was declared by the authors.

Financial Disclosure: The authors declared that this study received no financial support.

References

1. Cohen SP. Sacroiliac joint pain: a comprehensive review of anatomy, diagnosis, and treatment. Anesth Analg. 2005;101:1440-53.
2. Tuite MJ. Sacroiliac joint imaging. Semin Musculoskelet Radiol. 2008;12:72-82.
3. Demir M, Mavi A, Gümüsburun E, Bayram M, Gürsoy S, Nishio H. Anatomical variations with joint space measurements on CT. Kobe J Med Sci. 2007;53:209-17.
4. Tok Umay S, Korkmaz M. Frequency of anatomical variation of the sacroiliac joint in asymptomatic young adults and its relationship with sacroiliac joint degeneration. Clin Anat. 2020;33:839-43.
5. Kaiser SP, Gardner MJ, Liu J, Routt ML Jr, Morshed S. Anatomic determinants of sacral dysmorphism and implications for safe iliosacral screw placement. J Bone Joint Surg Am. 2014;96:e120.
6. Mendel T, Noser H, Kuervers J, Goehre F, Hofmann GO, Radetzki F. The influence of sacral morphology on the existence of secure S1 and S2 transverse bone corridors for iliosacroiliac screw fixation. Injury. 2013;44:1773-9.
7. Navallas M, Ares J, Beltrán B, Lisbona MP, Maymó J, Solano A. Sacroiliitis associated with axial spondyloarthropathy: new concepts and latest trends. Radiographics. 2013;33:933-56.
8. Wagner D, Ossendorf C, Gruszka D, Hofmann A, Rommens PM. Fragility fractures of the sacrum: how to identify and when to treat surgically? Eur J Trauma Emerg Surg. 2015;41:349-62.
9. Teran-Garza R, Verdines-Perez AM, Tamez-Garza C, et al. Anatomical variations of the sacro-iliac joint: a computed tomography study. Surg Radiol Anat. 2021;43:819-25.
10. Postacchini R, Trasimeni G, Ripani F, Sessa P, Perotti S, Postacchini F. Morphometric anatomical and CT study of the human adult sacroiliac region. Surg Radiol Anat. 2017;39:85-94.
11. Prassopoulos PK, Faflia CP, Voloudaki AE, Gourtsoyiannis NC. Sacroiliac joints: anatomical variants on CT. J Comput Assist Tomogr. 1999;23:323-7.
12. Fortin JD, Ballard KE. The frequency of accessory sacroiliac joints. Clin Anat. 2009;22:876-7.
13. Jurik AG, Herregods N. The sacroiliac joint across ages - what is normal? Ther Adv Musculoskelet Dis. 2024;16:1759720X241241126.
14. Ziegeler K, Ulas ST, Poddubnyy D, et al. Anatomical variation of the sacroiliac joint carries an increased risk for erosion and bone marrow oedema in axial spondyloarthritis. Rheumatology (Oxford). 2023;62:1117-23.
15. Kiil RM, Jurik AG, Zejden A. Anatomical variation at the sacroiliac joints in young adults: estimated prevalence by CT and concomitant diagnostics by MRI. Skeletal Radiol. 2022;51:595-605.
16. Ziegeler K, Kreutzinger V, Diekhoff T, et al. Impact of age, sex, and joint form on degenerative lesions of the sacroiliac joints on CT in the normal population. Sci Rep. 2021;11:5903.
17. Trentadue TP, Anderson TL, Wenger DE, McKenzie GA. Prevalence of accessory sacroiliac joint anatomy and associated clinical features. Skeletal Radiol. 2023;52:1359-68.
18. El Rafei M, Badr S, Lefebvre G, et al. Sacroiliac joints: anatomical variations on MR images. Eur Radiol. 2018;28:5328-37.
19. Trotter M. Accessory sacroiliac articulations in East African skeletons. Am J Phys Anthropol. 1964;22:137-41.
20. Malghem J, Vande Berg B, Lecouvet F, Koutaissoff S, Maldague B. Principes d'interpretation de l'imagerie des articulations sacro-iliaques [Principles of analysis for sacroiliac joints imaging]. JBR-BTR. 2007;90:358-67.
21. Poilliot AJ, Zwirner J, Doyle T, Hammer N. A systematic review of the normal sacroiliac joint anatomy and adjacent tissues for pain physicians. Pain Physician. 2019;22:E247-74.
22. Badr S, Khizindar H, Boulil Y, Abou Diwan R, Demondion X, Cotten A. Anatomical variants of the sacroiliac joint. Semin Musculoskelet Radiol. 2023;27:221-5.
23. Braun J, Sieper J, Bollow M. Imaging of sacroiliitis. Clin Rheumatol. 2000;19:51-7.
24. Oostveen JC, van de Laar MA. Magnetic resonance imaging in rheumatic disorders of the spine and sacroiliac joints. Semin Arthritis Rheum. 2000;30:52-69.
25. Zappia M, Maggialetti N, Natella R, et al. Diagnostic imaging: pitfalls in rheumatology. Radiol Med. 2019;124:1167-74.

RESEARCH ARTICLE

DOI: 10.4274/AdvRadiolImaging.galenos.2024.65375
Adv Radiol Imaging 2025;2(1):5-7

Tomographic Assessment of Normal Abdominal Muscle Thickness Values in Adolescents

Hatice Kübra Özdemir, Ayşegül Kayhan

Konya City Hospital, Clinic of Radiology, Konya, Türkiye

Abstract

Objectives: The transversus abdominis (TA), internal oblique (IO), and external oblique (EO) muscles comprise the three layers of the abdominal muscles. These muscles contribute to body stability. In the early stages of muscular diseases, low back pain may manifest. The purpose of this study was to use computed tomography (CT) to determine the normal thickness of specific abdominal muscles in adolescents.

Methods: Muscle thickness was measured from a section passing through the umbilicus during CT examination performed for other reasons on 500 adolescent children aged 12-18 years.

Results: The average muscle thickness was greater in boys (mean=28.8, p=0.30). The thickest muscle was the IO in both sexes. Muscle thickness was the thickest in the IO in both genders. Muscle thickness was positively correlated with body mass index (p=0.001).

Conclusion: Understanding the normal thickness of abdominal muscles can guide diagnosis and treatment. Muscle thicknesses are as follows: IO, EO, and TA.

Keywords: Abdominal muscle thickness, normal, computed tomography, adolescent

Introduction

The abdominal muscle planes comprise the lateral abdominal muscles, transversus abdominis (TA), internal oblique (IO), and external oblique (EO) compartments. These muscle structures play a role in body stability. Muscle diseases can present clinically as low back pain. When the previous literature was examined, muscle disease involvement was observed in all age groups. The normal values of muscle diseases in pediatric patients are important for early diagnosis.[1,2]

Ultrasonography (US), magnetic resonance imaging (MRI), and computed tomography (CT) are the basic imaging methods for assessing muscle tissue. US is the most appropriate examination for pediatric patients because of the lack of radiation and cost. However, in some clinics, access to US can be more difficult than access to cross-sectional examination. In addition, in some clinics, muscle planes can be evaluated incidentally in cross-sectional examinations for other reasons. Therefore, measuring the thickness of muscle planes using cross-sectional methods and knowing their normal values in pediatric patients can provide early diagnosis in the future.[2-4]

When the literature data are examined, Rahmani et al.[1] and Aydin and Fatihoğlu,[2] it is understood that the studies are mostly conducted on adult populations. Muscle measurement data obtained via CT examination in adolescents are limited. In our study, we aimed to make measurements by standardizing muscle plans in a certain cross-sectional plane with a CT examination performed for another purpose.

Methods

This retrospective study was approved by the Gülhane Faculty of Medicine Ankara Training and Research Hospital Clinical Research Ethics Committee approval (decision no: AEAH-KAEK-2021/12-15377834.11, date: 07.12.2021). Informed consent was not possible because of the decision's retrospective character.

A total of 520 CT scans performed for other reasons between January 2022 and December 2023 among patients aged 12-18 were retrospectively included in our study. Regardless of whether the examination was contrasted or not, patients with a history of neuromuscular, rheumatological, dermatological, or systemic disease or a history of surgery were excluded from the study. The study included 500 participants who satisfied the exclusion criteria.

The axis perpendicular to the anterior posterior line, which passes through most lateral muscle planes in the axial series and crosses the umbilicus level, was used for the measurement. Both sides of the measurement were measured. The patient's age, gender, and body mass index were also assessed. An example measurement is shown in Figure 1.

Cite this article as: Özdemir HK, Kayhan A. Tomographic assessment of normal abdominal muscle thickness values in adolescents. Adv Radiol Imaging. 2025;2(1):5-7

Address for Correspondence: Hatice Kübra Özdemir MD, Konya City Hospital, Clinic of Radiology, Konya, Türkiye
E-mail: haticekubra86@gmail.com ORCID ID: orcid.org/0000-0003-4387-5811
Received: 15.09.2024 Accepted: 23.12.2024 Epub: 08.01.2025 Published: 30.04.2025

After scouts were acquired, imaging was performed while supine using the following parameters: rotation time=0.33 s, 80/120 Sn kVp, 60 mAs, and cranio-caudal scanning. The slice is 1.5-mm thick. Three planes were used for image reconstruction: axial, coronal, and sagittal.

Statistical Analysis

The Kolmogrov-Smirnov test was employed to evaluate the distribution's normality. To examine the variations in the t-test between the right and left sides, a paired t-test was employed. The Student's t-test was used to evaluate distinctions between males and females. The relationship between abdominal muscle thickness and body mass index (BMI), sex, age, and subcutaneous fat thickness (SFT) was assessed using the Pearson correlation coefficient test. $P<0.05$ on a 2-tailed scale was regarded as statistically significant.

Results

In our study population, the mean age was calculated as 14.55±3.2 years. The mean age of the girls was 15.2±2.5 years, while the mean age of the boys was 15.1±2.1 years. As expected, BMI was significantly higher in boys (p=0.16, Table 1).

The order of thickness of the three defined muscle tissues was the same in both genders. The thickest muscle is the IO, the EO is the medium-sized muscle, and the TA is the small muscle. No significant difference was observed in the measurement of right or left muscle thickness. Subcutaneous fat tissue did not differ between the groups (p=0.001). Average muscle tissue thickness and subcutaneous fat tissue measurements are presented in Table 2.

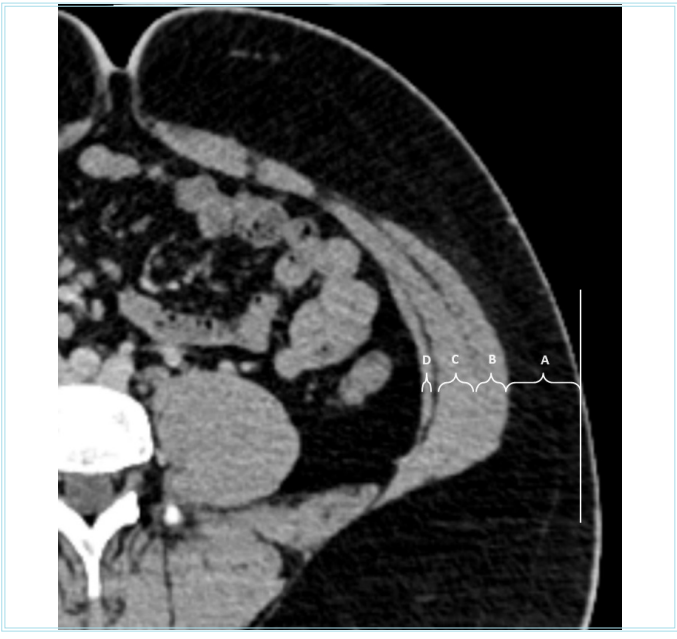

Figure 1. A) Subcutaneus fat thickness. B) External oblique muscle. C) Internal oblique muscle. D) Transversus abdominis muscle

Table 1. A statement indicating the comparison of age and BMI between sexes

Gender-variables		Mean±SD	p value
Boys (n=250)	Age (year)	15.1	0.16
	BMI (kg/m²)	28.8	0.30
Girls (n=250)	Age (year)	15.2	0.15
	BMI (kg/m²)	22.2	0.33

SD: Standard deviation, BMI: Body mass index

No significant correlation was observed between age and muscle thickness in any of the three muscle planes (p>0.5). No significant correlation was observed between SF measurement and age (p=0.548). We found a favorable association between BMI values and SFT values (IO, EO, and TA muscle thicknesses) (p<0.5). Correlations of muscle measurements with age and BMI are presented in Table 3.

Discussion

The normal dimensions of the abdominal muscle planes are important for the detection of back pain or disability. The normal dimensions of the abdominal muscle should be known so that pathological conditions can be revealed.[5] In this study, we aimed to determine the normative values of normal abdominal muscle planes in adolescence. There are limited studies on this subject in the literature. In the most recent literature, Aydin and Fatihoğlu,[2] found that muscles were thicker in the male population, which is consistent with our study. In addition, similar results were obtained in the study by Rahmani et al.[1] in the literature. As observed in all studies, no difference was observed between the right and left measurements in our study.

In accordance with the literature, the muscle thickness was similar in our study. Accordingly, the thickest muscle was the IO, the median muscle was the EO, and the thinnest muscle was the TA. However, there is no standardized method in the literature regarding where the muscle should be measured. In ultrasound examinations, localization is made by reporting the anterior axillary line and the iliac bone localization. This level is more inferior than our level. In our study, muscle thickness was observed to be more superiorly localized than other measurements in the literature due to the standard section of the level passing through

Table 2. Comparison of muscle planes by sex with the average of both sides

Gender (n=250)	Muscle measurements	Mean±SD (mm)
Boys	Transversus abdominis	5.5±0.9
	Internal oblique	13±1.1
	External oblique	10±0.8
	Subcutaneous fat thickness	9.5±0.6
Girls	Transversus abdominis	4.9±0.5
	Internal oblique	11±0.8
	External oblique	9±0.8
	Subcutaneous fat thickness	9.6±0.6

SD: Standard deviation

Table 3. Correlation of muscle mass with age and BMI

	Age		BMI	
	r	p value	r	p value
Mean TA	-0.059	0.548	0.398	0.001
Mean IO	-0.060	0.538	0.418	0.001
Mean EO	-0.065	0.648	0.338	0.001
Mean SFT	-0.258	0.548	0.378	0.001

TA: Transversus abdominis, IO: Internal oblique, EO: External oblique, SFT: Subcutaneous fat thickness, BMI: Body mass index

the umbilicus. For this reason, the muscle plane thickness was reported to be thicker than that reported by Aydin and Fatihoğlu.[2]

Since studies in the literature are generally conducted on the adult population, a negative correlation has been found between muscle thickness and age. In the present study, no significant relationship was observed between age and muscle thickness. Because the study was conducted on adolescents, our population has a growing structure, and it is naturally accepted that atrophy findings are not observed with age. In addition, the literature mentions the low negative correlation in measurements because the TA muscle planes consist of type 2 fibers, but such a relationship was not observed in our study. In future studies, new study topics can be determined by analyzing the muscle dimension growth by analyzing subgroups according to pediatric and adolescent age.[6,7]

We found a positive correlation between BMI values and all muscle planes and fat tissue. In the study by Aydin and Fatihoğlu,[2] a positive correlation was observed between all muscle planes except the EO and height. Springer et al.[8] found a positive correlation between BMI, as in our study. Our study was similar to that of Springer et al.[8] However, the use of only BMI values in our study prevented detailed analysis specific to height or weight.

Pediatric group measurements differ from adult measurements because of the muscle growth pattern. Knowing the normal values can provide information about possible future musculoskeletal disorders and low back pain. In addition, since there may be differences in follow-up among the athlete population, this can provide information about the degree of hypertrophy. Our study can provide a standard normogram measurement that provides convenience in terms of measurement location, such as the umbilicus.

Study Limitations

There are some limitations to our study. Our study cannot provide a detailed analysis of children aged below 12 years. This is only for the adolescent period. Differences between observers among radiologists were not measured. Due to the insufficient number of MRI examinations, CT examinations were mostly performed in the emergency department. MRI examination would be a more appropriate examination due to soft tissue resolution. Although patients with normal imaging findings from CT examinations performed for any reason were included in the study, the fact that CT was not performed retrospectively from a completely normal population may have misled the findings. Because CT cannot be performed as a priority in future screenings for muscle diseases due to radiation, the rate of diagnosis may be low in patients with this suspicion.

Conclusion

As a result, knowing the normal values of abdominal muscle planes in adolescence can provide information for the diagnosis of low back pain or muscle diseases. It is positively correlated with BMI. The muscle dimensions were determined as the thickest IO, median EO, and thinnest TA.

Ethics

Ethics Committee Approval: This study was approved by the Gülhane Faculty of Medicine Ankara Training and Research Hospital Clinical Research Ethics Committee approval (decision no: AEAH-KAEK-2021/12-15377834.11, date: 07.12.2021).

Informed Consent: Since the study was a retrospective study, informed consent was not required by the ethics committee.

Footnotes

Authorship Contributions

Surgical and Medical Practices - Concept - Design - Data Collection or Processing - Analysis or Interpretation - Literature Search - Writing: H.K.Ö., A.K.

Conflict of Interest: No conflict of interest was declared by the authors.

Financial Disclosure: The authors declared that this study received no financial support.

References

1. Rahmani N, Mohseni-Bandpei MA, Salavati M, Vameghi R, Abdollahi I. Comparative study of abdominal muscle thickness on ultrasonography in healthy adolescents and patients with low back pain. J Ultrasound Med. 2018;37:905-12.
2. Aydin S, Fatihoğlu E. Normal abdominal muscle thicknesses in adolescents: a sonographic study. Abant Med J. 2018;7:89-93.
3. Moncer R, Jemni S, Frioui S, Toulgui E, BelHadjYoussef I, Khachnaoui F. Cross-sectional study of low-back pain (LBP) in children and adolescents: prevalence and risk factor. Ann Phys Rehabil Med. 2016;59:e96.
4. Hill JJ, Keating JL. Daily exercises and education for preventing low back pain in children: cluster randomized controlled trial. Phys Ther. 2015;95:507-16.
5. Bayartai ME, Määttä J, Karppinen J, et al. Association of accelerometer-measured physical activity, back static muscular endurance and abdominal obesity with radicular pain and non-specific low back pain. Sci Rep. 2023;13:7736.
6. Airaksinen O, Brox JI, Cedraschi C, et al; COST B13 Working Group on Guidelines for Chronic Low Back Pain. Chapter 4. European guidelines for the management of chronic nonspecific low back pain. Eur Spine J. 2006;15(Suppl 2):S192-300.
7. Kiesel KB, Underwood FB, Mattacola CG, Nitz AJ, Malone TR. A comparison of select trunk muscle thickness change between subjects with low back pain classified in the treatment-based classification system and asymptomatic controls. J Orthop Sports Phys Ther. 2007;37:596-607.
8. Springer BA, Mielcarek BJ, Nesfield TK, Teyhen DS. Relationships among lateral abdominal muscles, gender, body mass index, and hand dominance. J Orthop Sports Phys Ther. 2006;36:289-97.

RESEARCH ARTICLE

DOI: 10.4274/AdvRadiolImaging.galenos.2025.98608
Adv Radiol Imaging 2025;2(1):8-13

Diagnostic Value of Apparent Diffusion Coefficient in Differentiating Benign and Malignant Focal Liver Lesions

Elnur Aliyev[1], Kemal Niyazi Arda[1], Mustafa Koyun[2]

[1]*University of Health Sciences Türkiye, Gülhane Training and Research Hospital, Clinic of Radiology, Ankara, Türkiye*
[2]*Kastamonu Training and Research Hospital, Clinic of Radiology, Kastamonu, Türkiye*

Abstract

Objectives: This study aims to evaluate the effectiveness of the apparent diffusion coefficient (ADC) in differentiating benign and malignant focal liver lesions (FLLs).

Methods: This study was conducted retrospectively on 87 patients who underwent liver magnetic resonance imaging (MRI). MRI of the patients was performed using a 1.5 Tesla Philips Intera MRI scanner. All ADC values of the lesions were measured using Radiant DICOM viewer software. The chi-square test, independent samples t-test, Mann-Whitney U test, and receiver operating characteristic analysis were used for statistical analysis.

Results: The patients included in the study were between 19 to 81 years of age, with a mean age of 52.6 (±14) years. While 51.7% (n=45) of the patients were female, 48.3% (n=42) were male. Benign lesions were detected in 54% (n=47) of the patients, while malignant lesions were found in 46% (n=40). The mean ADC values of malignant lesions were measured as $(0.95\pm0.37)\times10^{-3}$ mm²/s, and the mean ADC values of benign lesions were $(1.91\pm0.48)\times10^{-3}$ mm²/s, with a statistically significant difference between them ($p<0.001$). No statistically significant difference was found between the mean ADC values of hepatocellular carcinomas and metastases ($p=0.093$). The mean ADC value of focal nodular hyperplasias was calculated to be $(1.24\pm0.16)\times10^{-3}$ mm²/s, and the mean ADC value of hemangiomas was $(1.96\pm0.46)\times10^{-3}$ mm²/s, with a statistically significant difference between them ($p=0.012$). The optimal threshold value of ADC in distinguishing malignant lesions from benign ones was determined as 1.33×10^{-3} mm²/s, with a sensitivity of 93% and a specificity of 90% (area under the curve=0.959±0.019, $p<0.001$).

Conclusion: ADC measurements, being an easily applicable and reproducible method, can effectively contribute to differentiating between benign and malignant liver lesions.

Keywords: Apparent diffusion coefficient, diffusion magnetic resonance imaging, focal liver lesion, magnetic resonance imaging

Introduction

Focal liver lesions (FLLs) are defined as lesions with distinct borders in the liver parenchyma; which may be of benign or malignant origin. Benign lesions include hemangioma, adenoma, and focal nodular hyperplasia (FNH), while malignant lesions include hepatocellular carcinoma (HCC), cholangiocarcinoma (CCA), and metastases.[1] Accurate differentiation of benign and malignant lesions is critical for early treatment planning and improving prognosis. In addition, accurate differentiation of lesions is important to prevent unnecessary invasive interventions in benign lesions.

Imaging methods play a crucial role in the diagnosis of FLLs. Ultrasonography, computed tomography, and magnetic resonance imaging (MRI) are commonly used methods for evaluating the morphological and functional characteristics of these lesions.[2] MRI particularly stands out in revealing different tissue characteristics with its soft tissue contrast and various sequences.[3,4] Furthermore, the ability to perform hepatobiliary phase studies with gadolinium contrast agents provides additional diagnostic superiority over MRI.[5] Among MRI sequences, diffusion-weighted imaging (DWI) has an important application in radiology, particularly in cancer patients.[6] Moreover, DWI enables the evaluation of diffuse liver diseases and the assessment of malignant tumors' response to treatment.[7]

Apparent diffusion coefficient (ADC) measurements obtained from DWI provide parametric data about lesions.[7] ADC is a parameter that evaluates tissue density and microstructure by measuring the Brownian

Cite this article as: Aliyev E, Arda K, Koyun M. Diagnostic value of apparent diffusion coefficient in differentiating benign and malignant focal liver lesions. Adv Radiol Imaging. 2025;2(1):8-13

Address for Correspondence: Mustafa Koyun MD, Kastamonu Training and Research Hospital, Clinic of Radiology, Kastamonu, Türkiye
E-mail: dr.mustafakoyun@gmail.com **ORCID ID:** orcid.org/0000-0002-9811-4385
Received: 09.02.2025 **Accepted:** 08.04.2025 **Epub:** 18.04.2025 **Published:** 30.04.2025

motion of water molecules.[8] In DWI, ADC values can be quantitatively measured from tissues using at least two b-values.[9-11] ADC values are affected by factors such as cell density within tissue, intercellular space, necrosis areas, vascularity, and stromal structure.[3,5,8,12] Malignant lesions generally have denser cellular structures, limiting diffusion, which manifests as lower ADC values.[13-15] In contrast, benign lesions are associated with higher ADC values due to lower cell density and allowance for free movement of water molecules.[13-15] This difference suggests that ADC could be used as a biomarker in distinguishing benign from malignant lesions.

In the existing literature, the role of DWI and ADC values in characterizing normal tissues and various pathologies has been extensively studied.[16-19] Studies on the quantification of ADC values in FLLs have shown that this parameter can be used to differentiate between benign and malignant lesions.[6,13-15,20] However, some researchers have noted potential limitations regarding the diagnostic reliability of the method, reporting that overlap may be observed between ADC values of benign and malignant lesions.[14,21]

Despite advances in conventional MRI techniques, there remain significant diagnostic challenges in characterizing certain FLLs, particularly in cases where lesions demonstrate atypical enhancement patterns or in patients with chronic liver disease, where background parenchymal changes complicate interpretation. In these clinically ambiguous scenarios, ADC measurements can provide valuable additional information that may reduce the need for invasive diagnostic procedures such as biopsy. Furthermore, in patients with contraindications to contrast agents or in resource-limited settings where contrast-enhanced studies may not be readily available, ADC values could serve as an alternative diagnostic tool.

This study aims to investigate the diagnostic value of ADC in distinguishing between benign and malignant FLLs. In this context, the goal is to use ADC as a biomarker that can contribute to the clinical decision-making process.

Methods

Patient Selection

Patients included in our study were selected from those over 18 years of age who underwent dynamic liver MRI between March 2018 and March 2019. The inclusion criteria were determined as, complete dynamic liver MRI including DWI and ADC sequences, presence of FLL larger than 1 cm, and patient age above 18 years. Exclusion criteria were defined as: previous interventional procedures such as radiofrequency ablation of the liver lesion, history of local/systemic chemotherapy or radiotherapy treatment, and presence of artifacts in MRI that would limit evaluation. The FLLs initially planned to be included in the study were hemangioma, FNH, HCC, CCA, metastasis, and other rare liver lesions. Cysts were not included in the study as they are easily diagnosed. Pathology results were primarily considered in categorizing lesions into benign and malignant categories. Lesions without pathological diagnosis were categorized according to clinical and laboratory findings, as well as well-defined radiological imaging findings in the literature.[2,10] Consequently, using the inclusion and exclusion criteria, 87 patients were determined to be suitable for our study between the relevant dates. Patients' pathological diagnoses and demographic data were obtained from the hospital information management system.

MRI and ADC Measurements of Patients

All cases included in the study underwent dynamic liver MRI using a 1.5 Tesla Philips Intera MRI scanner (Philips Healthcare, Best, the Netherlands). The MRI sequences in the imaging protocol were as follows: T1 weighted, in/out phase, T1 weighted (THRIVE), T2 weighted single-shot, Heavy T2 weighted single-shot, and DWI SSH EPI (Table 1). The b-values used in DWI examinations were b=0 s/mm^2, 200 s/mm^2, and 800 s/mm^2. The THRIVE sequence was performed before gadolinium chelate administration and at 30, 70, and 300 seconds after administration.

The liver MRI images of patients meeting the research criteria were comprehensively evaluated by a radiologist with 3 years of experience. Appropriate diagnoses were assigned to detected FLLs based on well-defined radiological imaging characteristics in the literature and pathology results. Subsequently, ADC values of FLLs were measured. ADC measurements were performed using Radiant DICOM (Digital Imaging and Communications in Medicine) viewer software (version 2020.2.3, 64-bit, Medixant, Poznań, Poland). Region of interest (ROIs) of 0.5 cm^2 were used for ADC measurements (Figures 1, 2). During measurements, possible areas of necrosis and hemorrhage within the lesions were identified using other sequences (e.g., T2-weighted) and excluded from the ROI. Additionally, care was taken to exclude vascular structures, normal liver parenchyma, and artifacts from the ROIs. Three separate ADC measurements were made for each lesion, and their average was recorded in the data collection form as the final ADC value of the lesion.

Ethical Approval

Ethical approval for this retrospective study was obtained from the Non-interventional Research Ethics Committee of University of Health Sciences Türkiye (decision no: 18/319, date: 18.12.2018).

Table 1. Sequences used in dynamic liver MRI

Sequences	Description of the sequence
T1w in/out phase	Axial plane images were obtained in-phase and out-of-phase using T1-weighted 2-dimensional gradient echo technique with breath-hold protocol.
T1w (THRIVE)	T1-weighted three-dimensional gradient echo sequence with fat suppression was obtained using volumetric interpolation technique with breath-hold protocol.
T2w single-shot	Axial plane T2-weighted single-shot turbo spin-echo images were obtained using half Fourier technique.
Heavy T2w single-shot	T2-weighted images were obtained in the axial plane using half Fourier technique with single-shot turbo spin-echo sequence.
DWI SSH EPI	Diffusion-weighted images were obtained under free breathing using echo-planar imaging technique and single-shot method with b-values of 0, 200, and 800 s/mm^2.

w: Weighted, DWI: Diffusion-weighted imaging, SSH: Single-shot, EPI: Echo-planar imaging, THRIVE: T1 high-resolution isotropic volume examination, MRI: Magnetic resonance imaging

Statistical Analysis

In the study, continuous variables such as age and ADC values were expressed as means and standard deviations. Categorical variables such as gender were expressed as numbers and percentages (%). The Kolmogorov-Smirnov test was used to evaluate whether continuous variables conformed to a normal distribution. The chi-square test was used to evaluate relationships between categorical variables. To test the difference in ADC values between malignant and benign lesions, an independent samples t-test was used for groups showing normal distribution, and Mann-Whitney U test was used for groups not showing normal distribution. Receiver operating characteristic (ROC) curve analysis was performed to evaluate the diagnostic performance of ADC values in distinguishing between benign and malignant lesions. The area under the curve (AUC) was calculated using ROC analysis. A value of $p<0.05$ was accepted as the significance level in all statistical analyses. 95% confidence intervals (CI) were reported for estimated parameters. All analyses were performed using IBM Statistical Package for the Social Sciences 26 software (IBM Corporation, Armonk, NY, USA).

Results

The ages of the 87 patients included in the study ranged from 19 to 81 years, with a mean age of 52.6 years (±14 years). 21.8% (n=19) of the patients were between 19 and 40 years, 47.2% (n=41) were between 41 and 60 years, and 31% (n=27) were between 61 and 81 years.

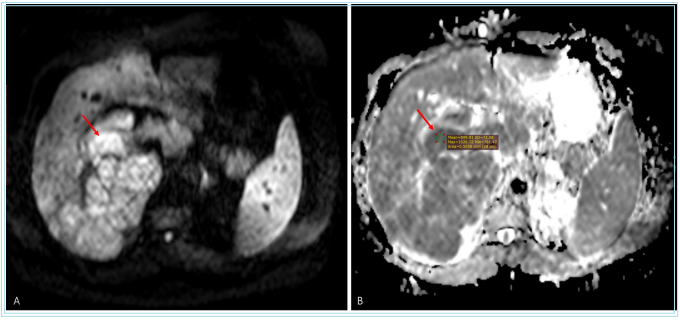

Figure 1. DWI (A) and ADC (B) images of a 46-year-old male patient with renal cell carcinoma metastasis in the liver. The lesion is localized in liver segment 7-8, appearing hyperintense on DWI and hypointense on ADC (arrow demonstrates an example ADC measurement)

DWI: Diffusion-weighted image, ADC: Apparent diffusion coefficient

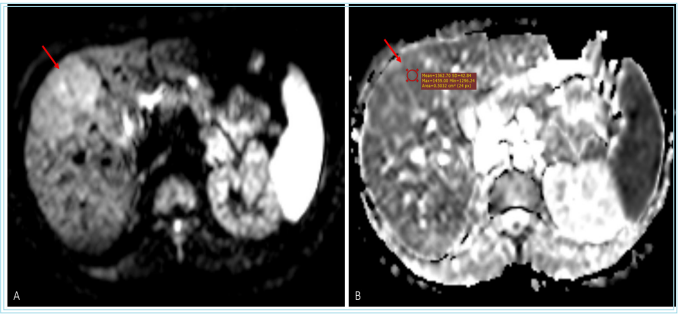

Figure 2. DWI (A) and ADC (B) images of a 19-year-old female patient with FNH in the liver. The lesion is localized in liver segment 8, appearing hyperintense on DWI and isointense on ADC (arrow demonstrates an example ADC measurement)

DWI: Diffusion-weighted image, ADC: Apparent diffusion coefficient, FNH: Focal nodular hyperplasia

When evaluated in terms of gender distribution, 51.7% (n=45) of the participants were female while 48.3% (n=42) were male (Table 2).

All malignant lesions (n=40) had a pathological diagnoses. Of these lesions, 82.5% (n=33) were metastases, 15% (n=6) were HCC, and 2.5% (n=1) was CCA. Among benign lesions (n=47), 6.4% (n=3) had a pathological diagnosis of FNH, while 93.6% (n=44) had a radiological diagnosis of hemangioma (Table 3).

The mean ADC value of all lesions in our study was measured as $(1.47\pm0.64)\times10^{-3}$ mm²/s. As a result of statistical analysis, the mean ADC value of malignant lesions was found to be $(0.95\pm0.37)\times10^{-3}$ mm²/s, which was significantly lower than the mean ADC value of benign lesions of $(1.91\pm0.48)\times10^{-3}$ mm²/s ($p<0.001$) (Table 4).

Accordingly, while the mean ADC value of 33 metastases was $(0.9\pm0.38)\times10^{-3}$ mm²/s, the mean ADC value of 6 HCCs was found to be $(1.18\pm0.21)\times10^{-3}$ mm²/s (Table 4). In the analysis performed with an

Table 2. Demographic characteristics of patients

Demographic characteristics, n=87		n (%)
Age, (19-81 years) Mean (±SD)=52.6 (±14)	19-40 years	19 (21.8)
	41-60 years	41 (47.2)
	61-81 years	27 (31)
Gender	Female	45 (51.7)
	Male	42 (48.3)
Total		87 (100)

SD: Standart deviation

Table 3. Distribution of focal liver lesions according to final diagnoses

	Lesion types	n (%)
Malign, n=40	Metastasis*	33 (82.5)
	HCC*	6 (15)
	CCA*	1 (2.5)
Benign, n=47	Hemangioma**	44 (93.6)
	FNH*	3 (6.4)
Total		87 (100)

*Diagnosis confirmed by pathological examination; **Diagnosis based on radiological imaging.
HCC: Hepatocellular carcinoma, CCA: Cholangiocellular carcinoma, FNH: Focal nodular hyperplasia

Table 4. Comparison of ADC values between benign and malignant lesions and their subtypes

	n (%)	ADC value, ($\times10^{-3}$ mm²/s)	p
		Mean (±SD)	
Benign	47 (54)	1.91 (±0.48)	**<0.001**
Malign	40 (46)	0.95 (±0.37)	
Metastasis	33 (82.5)	0.9 (±0.38)	0.093*
HCC	6 (15)	1.18 (±0.21)	
Hemangioma FNH	44 (93.6) 3 (6.4)	1.96 (±0.46) 1.24 (±0.16)	**0.012****
Total	87 (100)	1.47 (±0.64)	

*Independent samples t-test; **Mann-Whitney U test.
ADC: Apparent diffusion coefficient, HCC: Hepatocellular carcinoma, FNH: Focal nodular hyperplasia, SD: Standard deviation

independent samples t-test, no statistically significant difference was found between the ADC values of HCC and metastases (p=0.093). Due to the insufficient number of CCA (n=1, 2.5%), it was not included in the statistical comparison analyses. Among benign lesions, the mean ADC value of 44 hemangiomas was calculated as (1.96±0.46)×10^{-3} mm^2/s, which was higher than the mean ADC value of 3 FNHs, which was (1.24±0.16)×10^{-3} mm^2/s (Table 4). This difference was found to be statistically significant (p=0.012).

An ROC analysis was performed to evaluate the diagnostic performance of ADC values in distinguishing malignant from benign lesions (Figure 3). The optimal threshold value of ADC in distinguishing malignant lesions from benign ones was determined as 1.33×10^{-3} mm^2/s, and at this value, the sensitivity of the test was 93% and the specificity was 90%. The 95% CI of the obtained results ranges from 0.922 to 0.996. As a result of the analysis, the AUC was calculated as 0.959±0.019, and this value was found to be statistically significant (p<0.001).

Discussion

MRI is frequently used in clinical practice for detecting FLLs and shows a high success rate in diagnosis. However, MRI can sometimes be challenging in distinguishing between malignant and benign lesions. Our study demonstrates that ADC measurements can differentiate between malignant and benign FLLs and contribute to diagnosis. The most important results of our study are as follows. First, in our study, the mean ADC value of malignant lesions was found to be significantly lower than benign lesions. Second, using a threshold value of 1.33×10^{-3} mm^2/s resulted in high sensitivity and specificity values for distinguishing malignant lesions from benign ones. There is no significant difference between the mean ADC values of malignant lesion subtypes (metastasis and HCC). Among benign lesions, the mean ADC value of FNH is significantly lower than that of hemangiomas.

In our study, the mean ADC value of malignant lesions was found to be (0.95±0.37)×10^{-3} mm^2/s. This value is consistent with similar studies in the literature. Surov et al.[3] found the mean ADC values of malignant lesions to be (0.93±0.30)×10^{-3} mm^2/s, Battal et al.[22] (0.86±0.13)×10^{-3} mm^2/s, Demir et al.[23] (0.86±0.11)×10^{-3} mm^2/s, and Kim et al.[24] (1.01±0.38)×10^{-3} mm^2/s.

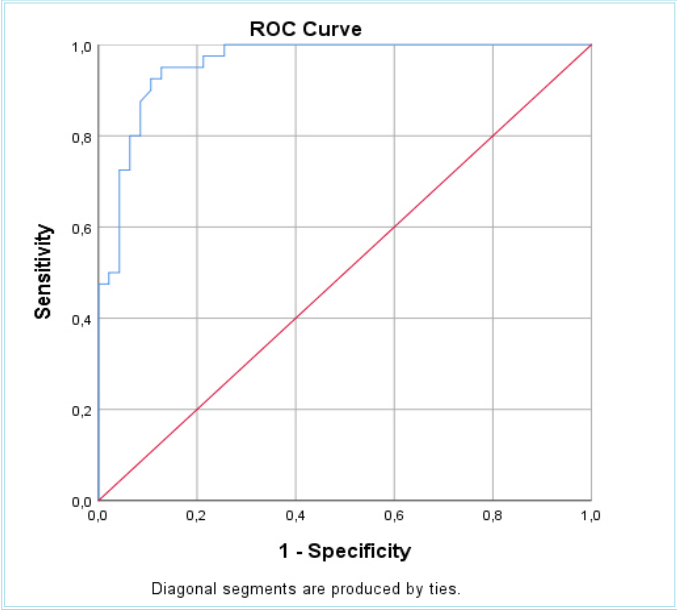

Figure 3. ROC analysis performed to evaluate the diagnostic ability of ADC values to distinguish malignant lesions from benign lesions

ROC: Receiver operating characteristic, ADC: Apparent diffusion coefficient

In our study, while the mean ADC value of metastases among malignant lesions was (0.9±0.38)×10^{-3} mm^2/s, the mean ADC value of HCCs was found to be (1.18±0.21)×10^{-3} mm^2/s, and no statistically significant difference was found between these values (p=0.093). Different results regarding ADC values of malignant lesions have been reported in comparative studies in the literature. Taouli et al.[10] reported ADC values as (0.94±0.6)×10^{-3} mm^2/s in metastases and (1.33±0.13)×10^{-3} mm^2/s in HCCs. In the study by Kim et al.,[24] ADC values were found to be (1.06±0.5)×10^{-3} mm^2/s in metastases and (0.97±0.31)×10^{-3} mm^2/s in HCCs. Similar to our study, the difference between mean ADC values of metastases and HCCs was not found to be statistically significant in the studies by Bruegel et al.,[7] Kim et al.,[24] Namimoto et al.,[25] and Kilickesmez et al.[26]

In our study, the mean ADC value of benign lesions was found to be (1.91±0.48)×10^{-3} mm^2/s, which was consistent with the value reported by Battal et al.[22] (1.94±0.61)×10^{-3} mm^2/s. Additionally, Kim et al.[24] reported mean ADC values of benign lesions as (2.49±1.39)×10^{-3} mm^2/s, and Jahic et al.[6] as 1.88 (1.326 to 2.48)×10^{-3} mm^2/s.

In our study, the mean ADC value of FNHs was found to be (1.24±0.16)×10^{-3} mm^2/s, which was statistically significantly lower than the mean ADC value of hemangiomas (1.96±0.46)×10^{-3} mm^2/s (p=0.012). ADC measurements were found to show excellent diagnostic performance in FNH-hemangioma differentiation. In previous studies, Cieszanowski et al.,[27] reported ADC values of hemangiomas as 1.55 (1.46-1.64)×10^{-3} mm^2/s, Taouli et al.,[10] as (2.95±0.67)×10^{-3} mm^2/s, and Gourtsoyianni et al.,[28] as 1.90 (1.56-2.24)×10^{-3} mm^2/s. In our study, the mean ADC value of hemangiomas falls between these values. In previous studies, Cieszanowski et al.[27] reported the mean ADC value of FNHs as 1.18 (0.99-1.36)×10^{-3} mm^2/s, Bruegel et al.[7] as (1.40±0.15)×10^{-3} mm^2/s, and Parikh et al.[29] as (1.49±0.49)×10^{-3} mm^2/s. In our study, the mean ADC value of FNHs falls between these reported values. Although FNHs are benign lesions, they can restrict diffusion due to their hypercellular internal structure, which emerges as one of the most important situations causing confusion in diagnosis.

In our study, the mean ADC values of malignant lesions were found to be significantly lower compared to benign lesions (p<0.001). In other studies in the literature, ADC values of malignant lesions are also significantly lower than those of benign lesions.[10,22,24,29]

In our ROC analysis, the optimal threshold value of ADC in distinguishing malignant lesions from benign ones was determined as 1.33×10^{-3} mm^2/s, with a sensitivity of 93% and a specificity, of 90% at this point. In the study by Battal et al.,[22] the threshold ADC value was found to be 1.21×10^{-3} mm^2/s, indicating that malignant lesions could be distinguished from benign ones with 100% sensitivity and 89.3% specificity at this value. In Parikh et al.'s[29] study, the threshold value was determined as 1.6×10^{-3} mm^2/s, stating that malignant lesions could be distinguished from benign ones with 74.2% sensitivity and 77.3% specificity. Possible reasons for reporting different threshold values in benign-malignant lesion differentiation in similar studies in the literature include imaging device, used sequence parameters, number of b-values taken, maximum b-factor, patient population, lesion sizes, and differences between observers.[30]

DWI has a wide range of clinical applications. It is not only a highly useful imaging method in detecting liver lesions, but also particularly stands out in detecting and monitoring ischemic stroke.[31,32] Besides these, it is used in the diagnosis of many malignancies such as brain tumors.[33] prostate cancer detection,[34] and rectal cancer detection.[35] In addition to tumor detection, DWI can also be used in tumor characterization and evaluation of treatment response.[9,36] Furthermore, DWI is a highly useful imaging method in distinguishing non-malignant lesions such as abscesses from cystic/necrotic tumors.[36]

Despite DWI's potential in tumor detection and characterization, there are various obstacles to its widespread use. These obstacles include a lack of standardization in imaging protocols, such as the b-values used, and difficulties in evaluating tumor heterogeneity.[9] Additionally, differences between evaluators can be considered another obstacle.[9] To overcome these limitations, integration of ADC measurements into routine clinical practice should be strongly encouraged, supported by clearly defined threshold values. Based on our findings, we recommend using the threshold value of 1.33×10^{-3} mm^2/s as a complementary diagnostic tool, especially when conventional imaging findings are ambiguous. However, ADC values must always be interpreted alongside other imaging findings and clinical context due to possible overlaps between pathologies such as FNH and HCC. Most importantly, the establishment of standardized acquisition protocols with consistent b-values across different MRI systems and institutions is crucial. Such standardization would significantly enhance reproducibility, facilitate reliable comparisons of ADC measurements between centers, and ultimately improve the diagnostic accuracy and clinical utility of this non-invasive biomarker for the characterization of FLLs. Increasing awareness and training among radiologists regarding ADC interpretation can further support effective implementation in daily practice.

Study Limitations

Our study has several limitations. The first limitation is the inability to evaluate lesions with low incidence, such as lymphoma, adenoma, and abscess, in our study. Second on the list is the inability to obtain pathological diagnoses of hemangiomas among benign lesions. However, the well-defined radiological findings of hemangiomas reduce the need for histopathological verification in diagnosing these lesions. Third, the exclusion of lesions smaller than 1 cm is another limitation of our study. This exclusion criterion prevents the evaluation of ADC's diagnostic potential in early-stage lesions, which is particularly important for timely detection of malignancies. Future studies should aim to include smaller lesions to assess the reliability and diagnostic accuracy of ADC measurements in these cases, while addressing technical challenges such as partial volume effects and motion artifacts that may affect the accuracy of such measurements. Additionally, the relatively small sample size of our study, particularly within specific subgroups of lesions, is an important limitation that may affect the generalizability of our findings. The presence of only one case of CCA necessitated its exclusion from statistical comparisons. Future studies should aim to include representation of different histopathological subtypes, particularly rare lesions like CCA, to enable more comprehensive statistical analyses, and potentially improve the diagnostic utility of ADC values across a wider spectrum of FLLs. Our results should be validated in larger, multi-center studies before being widely applied in clinical practice. Studies with larger sample sizes are needed to validate the results and establish more definitive diagnostic thresholds.

Conclusion

In conclusion, it has been determined that ADC, which is an easily applicable and reproducible method, can effectively assist distinguishing between benign and malignant focal lesions detected in the liver.

Ethics

Ethics Committee Approval: Ethical approval for this retrospective study was obtained from the Non-interventional Research Ethics Committee of University of Health Sciences Türkiye (decision no: 18/319, date: 18.12.2018).

Informed Consent: Because this was a retrospective study, informed consent was not required by the ethics committee.

Footnotes

Authorship Contributions

Concept: E.A., Design: E.A., Data Collection or Processing: E.A., Analysis or Interpretation: E.A., Literature Search: E.A., M.K., K.N.A., Writing: E.A., M.K., K.N.A.

Conflict of Interest: No conflict of interest was declared by the authors.

Financial Disclosure: The authors declared that this study received no financial support.

References

1. Venkatesh SK, Chandan V, Roberts LR. Liver masses: a clinical, radiologic, and pathologic perspective. Clin Gastroenterol Hepatol. 2014;12:1414-29.
2. Kahraman G, Haberal KM, Dilek ON. Imaging features and management of focal liver lesions. World J Radiol. 2024;16:139-67.
3. Surov A, Eger KI, Potratz J, Gottschling S, Wienke A, Jechorek D. Apparent diffusion coefficient correlates with different histopathological features in several intrahepatic tumors. Eur Radiol. 2023;33:5955-64.
4. Pankaj Jain T, Kan WT, Edward S, Fernon H, Kansan Naider R. Evaluation of ADCratio on liver MRI diffusion to discriminate benign versus malignant solid liver lesions. Eur J Radiol Open. 2018;5:209-14.
5. Calistri L, Castellani A, Matteuzzi B, Mazzoni E, Pradella S, Colagrande S. Focal liver lesions classification and characterization: what value do DWI and ADC have? J Comput Assist Tomogr. 2016;40:701-8.
6. Jahic E, Sofic A, Selimovic AH. DWI/ADC in differentiation of benign from malignant focal liver lesion. Acta Inform Med. 2016;24:244-7.
7. Bruegel M, Holzapfel K, Gaa J, et al. Characterization of focal liver lesions by ADC measurements using a respiratory triggered diffusion-weighted single-shot echo-planar MR imaging technique. Eur Radiol. 2008;18:477-85.
8. Le Bihan D. Apparent diffusion coefficient and beyond: what diffusion MR imaging can tell us about tissue structure. Radiology. 2013;268:318-22.
9. Koh DM, Collins DJ. Diffusion-weighted MRI in the body: applications and challenges in oncology. Am J Roentgenol. 2007;188:1622-35.
10. Taouli B, Vilgrain V, Dumont E, Daire JL, Fan B, Menu Y. Evaluation of liver diffusion isotropy and characterization of focal hepatic lesions with two single-shot echo-planar MR imaging sequences: prospective study in 66 patients. Radiology. 2003;226:71-8.
11. Goshima S, Kanematsu M, Kondo H, et al. Diffusion-weighted imaging of the liver: optimizing b value for the detection and characterization of benign and malignant hepatic lesions. J Magn Reson Imaging. 2008;28:691-7.
12. Aoyagi T, Shuto K, Okazumi S, et al. Apparent diffusion coefficient correlation with oesophageal tumour stroma and angiogenesis. Eur Radiol. 2012;22:1172-7.

13. Schmid-Tannwald C, Dahi F, Jiang Y, et al. DW-MRI of liver lesions: can a single ADC-value represent the entire lesion? Clin Radiol. 2014;69:492-8.

14. Nalaini F, Shahbazi F, Mousavinezhad SM, Ansari A, Salehi M. Diagnostic accuracy of apparent diffusion coefficient (ADC) value in differentiating malignant from benign solid liver lesions: a systematic review and meta-analysis. Br J Radiol. 2021;94:20210059.

15. Testa ML, Chojniak R, Sene LS, et al. Is DWI/ADC a useful tool in the characterization of focal hepatic lesions suspected of malignancy? PLoS One. 2014;9:101944.

16. Kazci O, Ece B. Magnetic resonance imaging assessment of normal ADC values of the parotid gland. Curr Res MRI. 2023;2:16-8.

17. Helenius J, Soinne L, Perkiö J, et al. Diffusion-weighted MR imaging in normal human brains in various age groups. Am J Neuroradiol. 2002;23:194-9.

18. Woo S, Beier SR, Tong A, Hindman NM, Vargas HA, Kang SK. Utility of ADC values for differentiating uterine sarcomas from leiomyomas: systematic review and meta-analysis. Am J Roentgenol. 2024;223:2431280.

19. Sepahdari AR, Politi LS, Aakalu VK, Kim HJ, Razek AA. Diffusion-weighted imaging of orbital masses: multi-institutional data support a 2-ADC threshold model to categorize lesions as benign, malignant, or indeterminate. AJNR Am J Neuroradiol. 2014;35:170-5.

20. Filipe JP, Curvo-Semedo L, Casalta-Lopes J, Marques MC, Caseiro-Alves F. Diffusion-weighted imaging of the liver: usefulness of ADC values in the differential diagnosis of focal lesions and effect of ROI methods on ADC measurements. MAGMA. 2013;26:303-12.

21. Miller FH, Hammond N, Siddiqi AJ, et al. Utility of diffusion-weighted MRI in distinguishing benign and malignant hepatic lesions. J Magn Reson Imaging. 2010;32:138-47.

22. Battal B, Kocaoglu M, Akgun V, et al. Diffusion-weighted imaging in the characterization of focal liver lesions: efficacy of visual assessment. J Comput Assist Tomogr. 2011;35:326-31.

23. Demir OI, Obuz F, Sağol O, Dicle O. Contribution of diffusion-weighted MRI to the differential diagnosis of hepatic masses. Diagn Interv Radiol. 2007;13:81-6.

24. Kim T, Murakami T, Takahashi S, Hori M, Tsuda K, Nakamura H. Diffusion-weighted single-shot echoplanar MR imaging for liver disease. Am J Roentgenol. 1999;173:393-8.

25. Namimoto T, Yamashita Y, Sumi S, Tang Y, Takahashi M. Focal liver masses: characterization with diffusion-weighted echo-planar MR imaging. Radiology. 1997;204:739-44.

26. Kilickesmez O, Bayramoglu S, Inci E, Cimilli T. Value of apparent diffusion coefficient measurement for discrimination of focal benign and malignant hepatic masses. J Med Imaging Radiat Oncol. 2009;53:50-5.

27. Cieszanowski A, Anysz-Grodzicka A, Szeszkowski W, et al. Characterization of focal liver lesions using quantitative techniques: comparison of apparent diffusion coefficient values and T2 relaxation times. Eur Radiol. 2012;22:2514-24.

28. Gourtsoyianni S, Papanikolaou N, Yarmenitis S, Maris T, Karantanas A, Gourtsoyiannis N. Respiratory gated diffusion-weighted imaging of the liver: value of apparent diffusion coefficient measurements in the differentiation between most commonly encountered benign and malignant focal liver lesions. Eur Radiol. 2008;18:486-92.

29. Parikh T, Drew SJ, Lee VS, et al. Focal liver lesion detection and characterization with diffusion-weighted MR imaging: comparison with standard breath-hold T2-weighted imaging. Radiology. 2008;246:812-22.

30. Do RK, Chandarana H, Felker E, et al. Diagnosis of liver fibrosis and cirrhosis with diffusion-weighted imaging: value of normalized apparent diffusion coefficient using the spleen as reference organ. Am J Roentgenol. 2010;95:671-6.

31. Eswaradass P, Appireddy R, Evans J, et al. Imaging in acute stroke. Expert Rev Cardiovasc Ther. 2016;14:963-75.

32. Nentwich LM. Diagnosis of acute ischemic stoke. Emerg Med Clin North Am. 2016;34:837-59.

33. Le Bihan D, Turner R, Douek P, Patronas N. Diffusion MR imaging: clinical applications. AJR Am J Roentgenol. 1992;159:591-9.

34. Hoeks CM, Barentsz JO, Hambrock T, et al. Prostate cancer: multiparametric MR imaging for detection, localization, and staging. Radiology. 2011;261:46-66.

35. Schurink NW, Lambregts DMJ, Beets-Tan RGH. Diffusion-weighted imaging in rectal cancer: current applications and future perspectives. Br J Radiol. 2019;92:20180655.

36. Shenoy-Bhangle A, Baliyan V, Kordbacheh H, Guimaraes AR, Kambadakone A. Diffusion weighted magnetic resonance imaging of liver: principles, clinical applications and recent updates. World J Hepatol. 2017;9:1081-91.

RESEARCH ARTICLE

DOI: 10.4274/AdvRadiolImaging.galenos.2025.65365
Adv Radiol Imaging 2025;2(1):14-9

Pediatric Left Ventricular Non-compaction Cardiomyopathy: Radiological and Echocardiographic Imaging Findings

Şükriye Yılmaz[1], Hasan Bulut[1], Özkan Kaya[2]

[1]*University of Health Sciences Türkiye, Ankara Etlik City Hospital, Clinic of Radiology, Ankara, Türkiye*
[2]*University of Health Sciences Türkiye, Ankara Etlik City Hospital, Clinic of Pediatric Cardiology, Ankara, Türkiye*

Abstract

Objectives: Non-compaction cardiomyopathy is a rare form characterized by the ventricular myocardium comprising an outer layer of normally compacted myocardium and an inner layer of non-compacted myocardium. The diagnosis primarily relies on imaging modalities, including echocardiography (ECHO) and cardiac magnetic resonance imaging. The aim of our study was to evaluate ECHO and cardiac magnetic resonance imaging findings in a group of children with isolated left ventricular non-compaction.

Methods: Between September 2022 and January 2025, pediatric patients under 18 years of age, who exhibited ECHO findings suggestive of left ventricle non-compaction, were retrospectively enrolled. Contrast-enhanced cardiac magnetic resonance imaging, including late gadolinium enhancement as well as two-chamber, four-chamber, and short-axis views, was performed to assess ventricular size, wall characteristics, and function in patients with suspected myocardial non-compaction based on ECHO findings.

Results: A total of 35 patients, with a median age of 14 years, were recruited. In the 12 patients where both ECHO and cardiac magnetic resonance imaging (cMRI) findings were concordant, leading to a definitive diagnosis on ECHO, the median non-compacted-to-compacted (NC/C) myocardial layer ratio in diastole was 2.6, while on cMRI, according to Petersen's criteria, the median NC/C ratio in end-diastole was 1.6.

Conclusion: ECHO is a reliable and non-invasive modality for monitoring left ventricular systolic function and wall characteristics. However, cardiac magnetic resonance imaging is recommended for a more precise assessment of left ventricular remodeling, right ventricular size and function, and the detection of myocardial fibrosis.

Keywords: Cardiomyopathy, left ventricular non-compaction, echocardiography, cardiovascular magnetic resonance imaging, children

Introduction

Non-compaction cardiomyopathy is a rare form of cardiomyopathy characterized by the ventricular myocardium comprising an outer layer of normally compacted myocardium and an inner layer of non-compacted myocardium.[1,2] The left ventricular myocardium consists of two distinct layers: a compact layer and a non-compact layer.[3] Non-compaction is traditionally associated with the left ventricle but may also involve the right ventricle as part of a biventricular presentation.[4,5] The American Heart Association (AHA) classifies left ventricular non-compaction (LVNC) as a genetic cardiomyopathy,[6] whereas the European Society of Cardiology categorizes it as a condition associated with other cardiomyophatie phenotypes (unclassified) and left ventricule hypertrabeculation.[7]

LVNC may present as an isolated condition or associated with congenital heart diseases, genetic syndromes, or neuromuscular disorders. This observation supports the notion that LVNC is not a distinct cardiomyopathy but rather a morphological manifestation of various underlying diseases.[1]

LVNC is often asymptomatic, but it can manifest with heart failure, arrhythmias, and thromboembolic events. Electrocardiography (ECG) abnormalities are more common in pediatric patients; however, they are non-specific.[2]

Although echocardiography (ECHO) and cardiac magnetic resonance imaging (cMRI) are widely utilized, the gold standard diagnostic criteria remain undefined due to the reversibility of the hypertrabecular structure and the variability in systolic and diastolic function findings among patients.[3] The diagnosis of LVNC is based on morphological criteria. ECHO is the primary diagnostic modality, and also essential for patient follow-up. cMRI with late gadolinium enhancement (LGE) is a complementary imaging tool that aids in confirming the diagnosis and provides prognostic insights.[8]

Cite this article as: Yılmaz Ş, Bulut H, Kaya Ö. Pediatric left ventricular non-compaction cardiomyopathy: radiological and echocardiographic imaging findings. Adv Radiol Imaging. 2025;2(1):14-9

Address for Correspondence: Şükriye Yılmaz MD, University of Health Sciences Türkiye, Ankara Etlik City Hospital, Clinic of Radiology, Ankara, Türkiye
E-mail: dryavuzer@gmail.com **ORCID ID:** orcid.org/0000-0002-5777-6147
Received: 12.02.2025 **Accepted:** 24.04.2025 **Published:** 30.04.2025

cMRI has gained increasing popularity in recent years as a diagnostic imaging modality due to its high-resolution anatomical detail. It allows for a comprehensive assessment of systolic and diastolic function, detection of myocardial fibrosis through LGE, and evaluation of ventricular wall structure and motion. Numerous studies have examined cMRI's diagnostic utility and criteria in identifying LVNC in adults.[2,5,9] These investigations consistently demonstrate the superiority of cMRI over ECHO, particularly in evaluating myocardial compaction in regions that are challenging to visualize with ECHO, such as the left ventricular apex and lateral wall.[9] In routine clinical practice, the most widely accepted cMRI-based diagnostic criterion for LVNC in adults is a non-compacted to compacted (NC/C) myocardium ratio of ≥2.3 during end-diastole, as established by Petersen et al.[10] in a cohort of patients aged 14 to 46 years. In contrast, limited research has explored the diagnostic role of cMRI in pediatric populations, and standardized diagnostic criteria for children have yet to be established.[3,8] The objective of the present study is to assess cMRI findings in pediatric patients with LVNC, to compare these with ECHO findings, and to evaluate the applicability of adult-based diagnostic criteria in a pediatric context, with the aim of proposing appropriate criteria for use in children.

Methods

Patients and Data Collection

From September 2022 to January 2025, pediatric patients with suspicious ECHO features for LVNC will be retrospectively screened and included in the study. Poor imaging quality, as well as congenital heart disease, other types of cardiomyopathies, or neuromuscular disorders in patients, were exclusion criteria for the study. cMRI images were evaluated for the presence of LVNC.

The cMRI, ECHO, and electrophysiological findings of patients with LVNC were recorded, as were the patients' demographic characteristics, clinical symptoms, and family history of cardiomyopathy and sudden cardiac death (SCD).

The study was approved by University of Sciences Türkiye, Ankara Etlik City Hospital's Clinical Research Ethics Committee (approval number: 2024-765, date: 02.12.2024).

Echocardiographic Imaging

ECHO imaging was performed using two-dimensional, Doppler, and M-mode ECHO. Parasternal long-axis and short-axis views, as well as apical two-chamber, three-chamber, and four-chamber views, were acquired. The criteria for inclusion in the study were an age of less than 18 years at the time of diagnosis and ECHO evidence of isolated LVNC, defined by ECHO measurements evaluated according to Pignatelli's criteria: (1) the presence of multiple ECHO trabeculations, (2) multiple deep intertrabecular recesses communicating with the ventricular cavity, as demonstrated by color Doppler imaging, with recesses observed in the apical or mid-ventricular regions, and (3) a two-layered myocardial structure with >1.4 at end diastole phase.[8] NC/C ratio was measured in the parasternal short-axis view during the end-diastolic phase at three locations within the posterior and posterolateral regions of the left ventricle (Figure 1).

Cardiac Magnetic Resonance Imaging

cMRI was conducted using a "1.5-T scanner (Ingenia Evolution, Philips Medical Systems, Best, The Netherlands)", equipped with a dedicated cardiac phased-array coil and ECG gating. Steady-state free precession CINE sequences were obtained in the short-axis, four-chamber, and two-chamber planes. LGE imaging was performed in both the short-axis and the 2- and 4-chamber planes, commencing 10 minutes after administering 0.1 mmol/kg of gadobutrol. Image analysis was performed using the Philips IntelliSpace Portal cardiac imaging software. cMRI was evaluated by two radiologists (Ş.Y, H.U.) with at least 5 years of experience in this field.

In the cMRI examination, axial, sagittal, and coronal white blood sequences were acquired in orthogonal planes to assess anatomical details. CINE imaging was performed in the two-chamber, four-chamber, and short-axis views to evaluate left ventricular ejection fraction (EF), end-diastolic volume (EDV), end-systolic volume (ESV), and ventricular wall structure. The endocardial and epicardial borders of the left ventricle were delineated in these phases to determine EDV and ESV for both ventricles, enabling the calculation of EF and stroke volume (SV). The assessment of NC/C myocardial layers was performed by measuring their thickness perpendicular to the compacted myocardium in the EDV using long-axis and short-axis views. Measurements excluded the 17th segment, in accordance with the AHA model. The highest NC/C ratio was recorded (Figure 2).

In this study, the thickness of the most hypertrophied myocardial segment in the mid-section of the interventricular septum was measured in both short-axis and long-axis images of patients with suspected LVNC. This assessment aimed to determine whether septal thickness could be a diagnostic parameter in suspected cases. EDV and ESV were indexed to

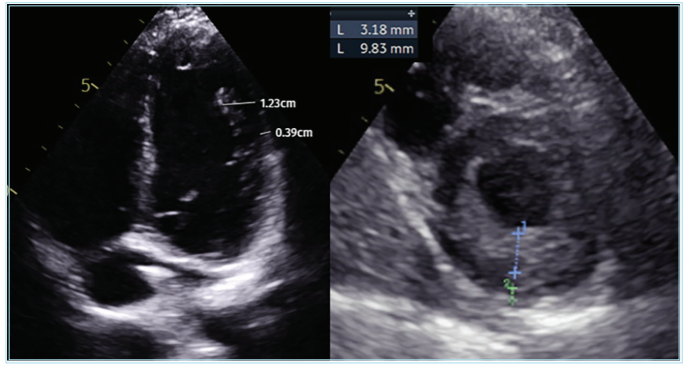

Figure 1. In echocardiographic images of the left ventricle, an increased non-compacted-to-compacted ratio was observed in measurements obtained during the end-diastolic phase, in the right long-axis and left short-axis views

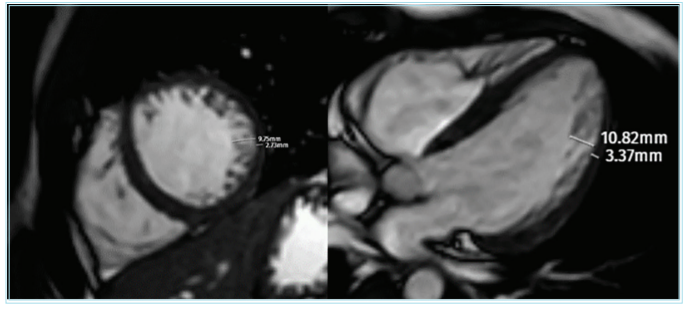

Figure 2. In cardiac magnetic resonance imaging images with white blood CINE imaging, an increased non-compacted-to-compacted ratio was observed in the left ventricular free wall, in the (right) short-axis and (left) long-axis views

the patient's body surface area to assess morphological abnormalities. They were compared with recently published normative values for children and adolescents, obtained using the same methodology.[11] In addition, all studies were visually evaluated for the presence of myocardial LGE.

Statistical Analysis

The distribution of all continuous variables was assessed using the Shapiro-Wilk test. Normally distributed variables are presented as mean±standard deviation, whereas non-normally distributed parameters are presented as median (interquartile range). The Pearson correlation coefficient was used to compare the LV non-compaction/compaction ratio between imaging modalities and to compare the cMRI non-compaction/compaction ratio with other findings. Statistical Package for the Social Sciences 26.0 (IBM, Chicago, IL, USA) was used to analyze all statistical data. A p value <0.05 was considered statistically significant.

Results

Clinical Findings

We reviewed the cMRI images of 32 patients, with ECHO features that were suspicious of LVNC. Due to technical problems and motion artifacts, 5 (16%) non-diagnostic examinations were excluded from the evaluation. In addition, 2 (6%) patients with congenital heart disease were excluded from the study. Thirteen (41%) patients did not meet the criteria for LVNC on cMRI. Demographic data for the 12 (38%) patients diagnosed with LVNC, confirmed through ECHO and CMR, were analyzed (Table 1).

Table 1. LVNC diagnosed patients' mean values of dermographic data

Baseline characteristics	n=12
Sex (boys/girls)	(12/6)
Age (years) median, IQR	15 (12.5-16)
Height (cm) mean±SD	161.5±19.9
Weight (kg) mean±SD	53.5±16.9
BMI (kg/m^2) mean±SD	20.1±3.3
BSA (m^2) mean±SD	1.53±0.34

LVNC: Left ventricular non-compaction, IQR: Interquartile range, SD: Standard deviation, BMI: Body mass index, BSA: Body surface area

The age range of patients with ECHO features suggestive of LVNC is 6-18 years, with a mean age of 14. Twenty patients (63%) were male, and 12 (37%) were female. The primary reasons for referral included clinical symptoms such as dyspnea (n=1), cardiac arrhythmias (n=4), chest pain (n=10), syncope (n=3), dizziness (n=3), heart murmur (n=2), as well as routine sports license evaluations (n=11) and a family history of cardiomyopathy or SCD. A total of 5 (16%) patients had a family history of early SCD of unknown etiology among first-degree relatives, while 3 (9%) patients had a diagnosis of dilated cardiomyopathy.

Electrocardiography and Ecocardiographic Findings

A total of 8 (25%) patients exhibited abnormal ECG findings, including incomplete right bundle branch block (n=2, 25%), atrioventricular block with sinus tachycardia (n=2, 25%), bradycardia (n=2, 25%), and ectopic beats (n=2, 25%). Among these, 1 (13%) patient with bradycardia had only ECHO abnormalities. All other patients with ECG abnormalities demonstrated positive findings for LVNC on both ECHO and cMRI.

Our study evaluated all 35 patients, who underwent cardiac cMRI based on ECHO findings. Among them, 10 patients had an NC/C ratio of 1-1.4 in the end-diastolic phase and were referred for cMRI due to high clinical suspicion. However, no pathological findings were detected on cMRI in these patients, and they were subsequently monitored. Additionally, among the 12 patients who met the diagnostic criteria on both cMRI and ECHO, mitral valve prolapse was identified in 3 patients, while 1 patient exhibited concomitant tricuspid and pulmonary insufficiency. No significant additional ECHO abnormalities were detected in the remaining patients.

Cardiac Magnetic Resonance Imaging Findings

In 13 patients with NC/C values of 1.4 or higher on ECHO (mean 1.6), while cMRI findings were negative the mean NC/C ratio measured on MRI was also 1.6. In contrast, 12 patients demonstrated positive findings for LVNC on both ECHO (mean NC/C 1.8) and cMRI (mean NC/C 2.6) (Table 2). LGE was not detected in any patient on cMRI.

Table 2. cMRI and echocardiographic findings in patients diagnosed with LVNC based on combined cMRI and echocardiographic evaluation

Patient no	Age	BMI	EDVI	ESVI	EF	IVS	ECHO NC/C	cMRI NC/C
1	15	22.4	62	21	67	7.5	3.1	3.6
2	12	15.4	20	19	68	6.1	1.5	2.5
3	16	21.6	63	26	63	7.7	1.7	2.3
4	16	22.2	90	36	60	5.3	1.4	2.9
5	15	20.9	80	36	59	5.6	1.6	2.6
6	14	26.7	77	38	62	4.6	2.6	2.7
7	18	17.3	64	20	69	6.7	1.8	2.7
8	15	22.1	55	23	58	4.5	1.8	2.7
9	16	19.1	61	29	62	6.1	1.7	2.4
10	8	20.8	43	16	76	6.6	1.4	2.3
11	8	16	45	18	64	6	1.5	2.3
12	15	16.6	104	34	55	5.6	1.9	3

cMRI: Cardiac magnetic resonance imaging, LVNC: Left ventricular non-compaction, BMI: Body mass index, EDVI: End diastolic volume index, ESVI: End systolic volume index, EF: Ejection fraction, IVS: Interventricular septum, ECHO: Echocardiography, NC/C: Non-compacted-to-compacted

Of the 12 patients who met the diagnostic criteria on both cMRI and ECHO, ECHO findings were similar in that mitral valve prolapse was observed in 3 patients. In contrast, 1 patient exhibited concomitant tricuspid and pulmonary insufficiency.

The NC/C ratios measured using ECHO correlate with those obtained through cMRI. This finding contrasts with a study conducted on adult patients, which reported a high degree of agreement between ECHO and cMRI measurements at end-diastole. Additionally, in the assessment of left heart function, EF, ESV, EDV, and SV, values indicated a mild reduction in left ventricular function in 3 of the 12 patients who met the definitive diagnostic criteria on cMRI (Table 3). In all examinations, a strong correlation was observed in NC/C ratios among patients who met the diagnostic criteria (Figure 3, Table 4).

Interventricular septum measurements were performed in LVNC patients to assess potential coexisting pathologies and their associations with other cardiomyopathies. Based on imaging studies conducted in these patients, no age-inappropriate abnormal septal thickness was detected.

Discussion

Although the classification of LVNC within the cardiomyopathy category remains a subject of debate among certain publishers and professional associations, ambiguities in its definition and diagnostic criteria do not dispute its clinical significance, as well as its disease progression, outcomes, and associated complications.[12]

LVNC can occur in both familial and sporadic forms. The familial recurrence rate in the pediatric population has been determined to be 50%, which is higher than that observed in the adult population.[13,14] In our study, genetic analysis was not conducted for family history; however, a family history of cardiac disease was identified in 25% of cases.

Table 3. cMRI and ECHO mean values for LVNC

ECHO and cMRI	Mean value
ECHO NC/C mean±SD	1.84±0.50
cMRI NC/C mean±SD	2.67±0.36
EDV (mL) mean, SD	105.5±29.06
ESV (mL) mean±SD	40.33±13.84
SV (mL) mean±SD	64.91±17.53
EDV/BSA (mL/m^2) mean±SD	67±12.68
ESV/BSA (mL/m^2) mean±SD	27.16±7.52
IVS (mm) mean±SD	6.02±1.01

cMRI: Cardiac magnetic resonance imaging, LVNC: Left ventricular non-compaction, ECHO: Echocardiography, SD: Standard deviation, EDV: End diastolic volume, ESV: End systolic volume, SV: Stroke volume, BSA: Body surface area, IVS: Interventricular septum

LVNC is more frequently observed in men, with reported prevalence ranging from 56% to 82%.[15,16] In the study conducted by Paszkowska et al.[17] on pediatric patients, the proportion of male patients diagnosed using cMRI was found to be 44%. In our study, this rate, with a male predominance, was determined to be 50% among a total of 12 patients who met the diagnostic criteria in both ECHO and cMRI examinations.

Abnormal ECG findings are frequently observed in pediatric patients with LVNC; however, they are often non-specific. Zuccarino et al.[18] reported that ECG changes may include ST-T abnormalities, bundle branch block, or Brugada-like ECG patterns. In the study conducted by Brescia et al.[19] on pediatric LVNC patients, arrhythmias were observed in 33.1% of 242 patients, with ventricular tachycardia identified in 17% of these cases. In our study, arrhythmias were observed in 7 out of 12 patients diagnosed with LVNC. Consistent with the literature, bundle branch block and sinus tachycardia were the most commonly detected arrhythmias. In the more advanced stages of LVNC, heart failure is observed in over 50% of patients.[5]

ECHO is the primary imaging method in cardiac evaluation in pediatric patients with its low cost, easy accessibility, and reproducibility.

In ECHO measurements studies, assessments have generally been conducted based on the Jenni criteria. However, these methods are employed as they are more suitable for pediatric patients.[7] Given that ECHO is a dynamic imaging modality with inherent subjectivity and operator dependence, cMRI correlation is particularly crucial in pediatric patients to ensure diagnostic accuracy and reliability.

In our study, in this context, 25 out of 35 patients met the diagnostic criteria based on ECHO evaluation, while 10 patients with high clinical suspicion underwent cMRI. Ultimately, 12 patients received a definitive

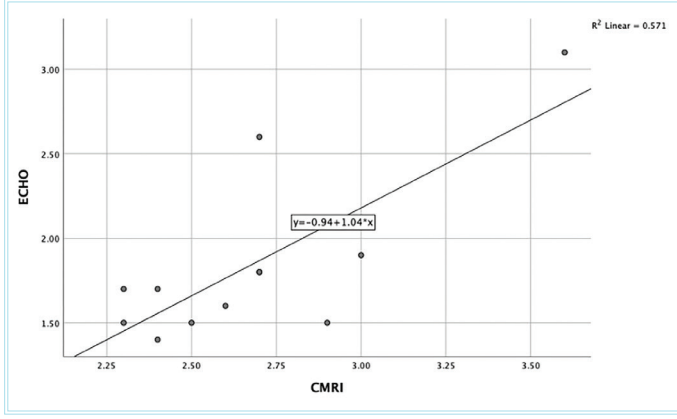

Figure 3. Non-compacted-to-compacted ratio cMRI and ECHO correlation analysis graph

ECHO: Echocardiography, cMRI: Cardiac magnetic resonance imaging

Table 4. Corelation between cMRI and ECHO

		ECHO NC/C	EDV	ESV	SV	EDV/BSA	ESV/BSA	EF	IVS
	Pearson r	**0.756***	0.20	0.13	0.23	0.217	0.064	0.08	0.05
cMRI NC/C	p	**0.004***	0.52	0.67	0.46	0.499	0.843	0.80	0.86
	n	**12**	12	12	12	12	12	12	12

*p<0.005.
cMRI: Cardiac magnetic resonance imaging, ECHO: Echocardiography, NC/C: Non-compacted-to-compacted, EDV: End diastolic volume, ESV: End systolic volume, SV: Stroke volume, BSA: Body surface area, EF: Ejection fraction, IVS: Interventricular septum

diagnosis based on the findings from both modalities. Notably, none of the 10 patients who could not be definitively diagnosed using ECHO met the diagnostic criteria on cMRI, which further demonstrates ECHO's diagnostic strength and reliability.

In the study conducted by Paszkowska et al.,[17] cMRI confirmed the diagnosis in 93% of children who exhibited LVNC features on ECHO. In our evaluation, this rate was measured as 48%.

Performing cMRI examination in all patients who meet the ECHO diagnostic criteria and are deemed highly suspicious for certain conditions is crucial for enhancing diagnostic accuracy. Additionally, it plays a significant role in patient follow-up, in treatment planning, and in identifying and monitoring comorbid conditions.

Our pediatric study compared ECHO images with those obtained via cMRI, both acquired at end-diastole to evaluate the NC/C ratio. The NC/C ratios measured using ECHO significantly correlated with those obtained through cMRI. This finding contrasts with a study conducted on adult patients, which reported a high degree of agreement between ECHO and cMRI measurements at end-diastole. This result is consistent with findings from a previous study conducted in pediatric patients.[1]

In the studies conducted by Grothoff et al.,[20] none of the cardiomyopathy patients exhibited LGE. In a cMRI study conducted on adult patients, which included a total of 47 individuals with LVNC, myocardial waves were detected in 40% of the patients, most frequently, in the mid-myocardial region.[21] In a study involving 25 pediatric patients, LGE was observed in 24% of cases, most commonly in the mid-myocardial region.[17] LGE was not detected in any of our patients. LGE represents fibrosis in these patients and can also indicate the possibility of suspected possible myocarditis. related. This rate is lower in pediatric patients than in others, possibly due to the relatively low development of fibrosis, which is attributed to the early onset of the disease.

In our study, the interventricular septum was measured at its thickest point in the midventricular region during the end-diastolic phase and assessed for its diagnostic contribution in patients with LVNC. Septal thickness was not found to exceed normal values in any of the diagnosed patients.

Study Limitations

This study is a single-center, retrospective analysis conducted over approximately three years at a large tertiary referral institution. As such, several limitations should be acknowledged. First, the sample size may limit the generalizability of the findings, as the characteristics of the study population may not be representative of broader or more diverse populations. Second, due to the retrospective design and the operator-dependent nature of ECHO assessments, a comprehensive analysis of diastolic function parameters and a more detailed evaluation of systolic function were not feasible. Finally, this study excluded patients under the age of six; consequently, assessment of noncompaction in this age group was not performed. This exclusion was due to the susceptibility of cardiac MRI sequences to motion artifacts, which are more prevalent in younger children.

Conclusion

cMRI is strongly recommended as a complementary imaging tool for assessing non-compaction, to accurately assess the extent of myocardial non-compaction and to evaluate ventricular size and systolic function reliably. To better understand the necessity and comparative value of ECHO and cMRI, further studies with larger patient cohorts are needed.

Ethics

Ethics Committee Approval: The study was approved by University of Health Sciences Türkiye, Ankara Etlik City Hospital's Clinical Research Ethics Committee (approval number: 2024-765, date: 02.12.2024).

Informed Consent: Because this was a retrospective study, informed consent was not required by the ethics committee.

Footnotes

Author Contributions

Surgical and Medical Practices: Ş.Y., Ö.K., Concept: Ş.Y., H.B., Design: Ş.Y., H.B., Ö.K., Data Collection or Processing: Ş.Y., Analysis or Interpretation: Ş.Y., H.B., Literature Search: Ş.Y., Ö.K., Writing: Ş.Y.

Conflict of Interest: No conflict of interest was declared by the authors.

Financial Disclosure: The authors declared that this study received no financial support.

References

1. Filho DCS, do Rêgo Aquino PL, de Souza Silva G, Fabro CB. Left ventricular noncompaction: new insights into a poorly understood disease. Curr Cardiol Rev. 2021;17:209-16.
2. Shi WY, Betancur MM, Nugent AW, et al. Long-term outcomes of childhood left ventricular no compaction cardiomyopathy: results from a national population-based study. Circulation. 2018;138:367-76.
3. Monda E, De Michele G, Diana G, et al. RETRACTED: left ventricular non-compaction in children: aetiology and diagnostic criteria. Diagnostics. 2024;4:115.
4. Ulusoy RE, Kucukarslan N, Kirilmaz A, Demiralp E. Noncompaction of ventricular myocardium involving both ventricles. Eur J Echocardiogr. 2006;7:457-60.
5. Towbin JA, Lorts A, Jefferies JL. Left ventricular non-compaction cardiomyopathy. Lancet. 2015;386:813-25.
6. Maron BJ, Towbin JA, Thiene G, et al. Contemporary Definitions and Classification of the Cardiomyopathies: An American Heart Association Scientific Statement from the Council on Clinical Cardiology, Heart Failure and Transplantation Committee; Quality of Care and Outcomes Research and Functional Genomics and Translational Biology Interdisciplinary Working Groups; and Council on Epidemiology and Prevention. Circulation. 2006:113;1807-6.
7. Arbelo E, Protonotarios A, Gimeno JR, et al. 2023 ESC Guidelines for the management of cardiomyopathies. Eur Heart J. 2023:44;3503-626.
8. Pignatelli RH, McMahon CJ, Dreyer WJ, et al. Clinical characterization of left ventricular noncompaction in children: a relatively common form of cardiomyopathy. Circulation. 2003;108:2672-8.
9. Choi Y, Kim SM, Lee SC, Chang SA, Jang SY, Choe YH. Quantification of left ventricular trabeculae using cardiovascular magnetic resonance for the diagnosis of left ventricular non-compaction: Evaluation of trabecular volume and refined semiquantitative criteria. J Cardiovasc Magn Reson. 2016;18:24.
10. Petersen SE, Selvanayagam JB, Wiesmann F, et al. Left ventricular non-compaction: insights from cardiovascular magnetic resonance imaging. J Am Coll Cardiol. 2005;46:101-5.

11. van der Ven JPG, Sadighy Z, Valsangiacomo Buechel ER, et al. Multicentre reference values for cardiac magnetic resonance imaging derived ventricular size and function for children aged 0–18 years. Eur Heart J Cardiovasc Imaging. 2020;21:102-13.

12. Krupickova S, Risch J, Gati S, et al. Cardiovascular magnetic resonance normal values in children for biventricular wall thickness and mass. J Cardiovasc Magn Reson. 2021;23:1.

13. Oechslin E, Jenni R. Left ventricular non-compaction revisited: a distinct phenotype with genetic heterogeneity? Eur Heart J. 2011;32:1446-56

14. Weiford BC, Subbarao VD, Mulhern KM. Noncompaction of the ventricular myocardium. Circulation. 2004;109:2965-71.

15. Finsterer J, Stöllberger C, Towbin JA. Left ventricular noncompaction cardiomyopathy: cardiac, neuromuscular, and genetic factors. Nat Rev Cardiol. 2017;14:224-37.

16. Stöllberger C, Finsterer J, Blazek G. Left ventricular hypertrabeculation/noncompaction and association with additional cardiac abnormalities and neuromuscular disorders. Am J Cardiol. 2002; 90:899-02.

17. Paszkowska A, Sarnecki J, Mirecka-Rola A, Kowalczyk-Domagała M, Mazurkiewicz Ł, Ziółkowska L. Imaging features of pediatric left ventricular noncompaction cardiomyopathy in echocardiography and cardiovascular magnetic resonance. J. Cardiovasc Dev Dis. 2022;9:77.

18. Zuccarino F, Vollmer I, Sanchez G, Navallas G, Pugliese F, Gayete A. Left ventricular noncompaction: imaging findings and diagnostic criteria. AJR Am J Roentgenol. 2015;204:519-30.

19. Brescia ST, Rossano JW, Pignatelli R, et al. Mortality and sudden death in pediatric left ventricular noncompaction in a tertiary referral center. Circulation. 2013;22:2202-8.

20. Grothoff M, Pachowsky M, Hoffmann J, et al. Value of cardiovascular MR in diagnosing left ventricular non-compaction cardiomyopathy and in discriminating between other cardiomyopathies. Eur Radiol. 2012;22:2699-709.

21. Wan J, Zhao S, Cheng H, et al. Varied distributions of late gadolinium enhancement found among patients meeting cardiovascular magnetic resonance criteria for isolated left ventricular non-compaction. J Cardiovasc Magn Reson. 2013;15:20.

CASE REPORT

DOI: 10.4274/AdvRadiolImaging.galenos.2025.99609
Adv Radiol Imaging 2025;2(1):20-3

Giant Bladder Diverticulum Presenting with Bilateral Inguinal Pain and Dysuria

Tuğba Çaviş[1], Cansu Bozkurt[1], Çetin Kocabıyık[2], Özgür Çınar[2], Selahattin Bedir[2], Kemal Niyazi Arda[1]

[1]*University of Health Sciences Türkiye, Gülhane Training and Research Hospital, Clinic of Radiology, Ankara, Türkiye*
[2]*University of Health Sciences Türkiye, Gülhane Training and Research Hospital, Clinic of Urology, Ankara, Türkiye*

Abstract

Bladder diverticulum is defined as the herniation of the bladder mucosa and submucosa through the muscular layer. Diverticula are usually asymptomatic and are often diagnosed incidentally. In this case report, we described a giant bladder diverticulum presenting with bilateral inguinal pain, dysuria, and palpable mass in the abdomen. Radiological imaging methods (ultrasonography, computed tomography, magnetic resonance imaging, voiding cystourethrography) were used for further evaluation along with laboratory examinations. After being diagnosed with giant bladder diverticulum, the patient underwent surgery. Postoperative control imaging methods were performed.

Keywords: Giant diverticulum, bladder diverticulum, diverticulectomy, radiology

Introduction

Bladder diverticulum is defined as the herniation of the bladder mucosa and submucosa through the muscular layer.[1] Bladder diverticula often occur secondary to bladder outlet obstruction, which causes high pressure in the bladder.[2] Diverticula are usually asymptomatic and are often diagnosed incidentally.[1] Symptomatic giant bladder diverticula may present with urinary retention, urinary tract infections, hematuria, abdominal mass, and abdominal pain.[3] The incidence of bladder diverticula is 1.7% in children and 1-6% in adults.[4] In the differential diagnosis of giant bladder diverticula, other abdominal cystic masses such as ovarian cysts, abscess, hematoma, and appendiceal mucocele should be considered. In this case report, we described a giant bladder diverticulum presenting with bilateral inguinal pain, burning sensation during urination, and palpable mass in the abdomen.

Case Report

A 64-year-old male presented to our center with complaints of a burning sensation during urination, pain in bilateral inguinal regions, and a palpable mass in the abdomen. On physical examination, there was a hard, palpable mass extending from the symphysis pubis to the epigastrium. During the physical examination, it was observed that the patient had tenderness in the suprapubic region. During the initial admission, laboratory data revealed C-reactive protein value of 72.5 mg/L (normal: 0-5 mg/L), hemoglobin value of 11.3 g/dL (normal: 11.9-15.4 g/dL), serum urea value of 49 mg/dL (normal: 18-55 mg/dL), and serum creatinine value of 0.9 mg/dL (normal: 0.7-1.2 mg/dL). Other laboratory values were within normal range. Radiological imaging methods were used for further evaluation along with laboratory examinations.

Abdominal ultrasonography (US) revealed bilateral grade 3 hydroureteronephrosis, more prominent on the left, a tortuous appearance in the left ureter, a large volume bladder with a double lumen appearance, and a trabeculated appearance on the bladder wall (Figure 1). The connection of both lumens could not be determined by ultrasound. Prostate volume was measured to be approximately 40 cc. Therefore, contrast-enhanced computed tomography (CT) was performed for further evaluation.

CT revealed a giant diverticulum measuring 15 x 9 x 14 cm (craniocaudal x transverse x anteroposterior) associated with the left lateral wall of the bladder. The diverticulum was connected to the bladder lumen by a narrow neck of 13 mm in diameter (Figure 2). The left ureter was observed between the diverticulum and the bladder, and had a tortuous appearance proximal to this level. The diverticulum had no connection with either ureterovesical junction.

With magnetic resonance imaging (MRI) urography a thin-walled diverticulum was observed, while there was a trabeculated appearance on the bladder wall (Figure 3). The narrow neck between the diverticulum and the bladder lumen was well demonstrated with MRI (Figure 3).

Cite this article as: Çaviş T, Bozkurt C, Kocabıyık Ç, Çınar Ö, Bedir S, Arda KN. Giant bladder diverticulum presenting with bilateral inguinal pain and dysuria. Adv Radiol Imaging. 2025;2(1):20-3

Address for Correspondence: Tuğba Çaviş MD, University of Health Sciences Türkiye, Gülhane Training and Research Hospital, Clinic of Radiology, Ankara, Türkiye
E-mail: tugbayayla86@yahoo.com **ORCID ID:** orcid.org/0000-0001-8878-9568
Received: 18.12.2024 **Accepted:** 05.02.2025 **Epub:** 19.03.2025 **Published:** 30.04.2025

Eventually, voiding cystourethrography (VCUG) was performed to evaluate the discharge of the diverticulum after micturition. A Foley catheter was inserted and contrast material was administered retrogradely. After administration of contrast material, anteroposterior and oblique images were obtained. Afterwards, the catheter was removed, and voiding phase images were obtained. Then, after waiting 30 minutes, the patient was again catheterized and the residual urine in the bladder and diverticulum was evaluated. The catheter was observed in the true bladder lumen on the right. Bladder trabeculation was increased; a giant diverticulum with smooth borders was seen on the left (Figure 4A). In the images taken after voiding, the amount of urine remaining in the bladder decreased significantly, while there was no significant difference in the amount of urine remaining in the diverticulum. In the images taken after re-catheterization, the bladder was completely emptied but a significant residue remained in the diverticulum (Figure 4B).

After being diagnosed with giant bladder diverticulum, the patient was operated on. We operated on our patient using an extravesical approach. This approach allowed identification and dissection of the diverticulum neck (Figure 5). In this patient, the left ureteral orifice was close to the bladder neck, so a double J catheter was placed in the left ureter intraoperatively. The patient was followed using a urethral catheter for 3 weeks. In the retrograde cystography taken in the third week, it was observed that there was no leakage outside the bladder; consequently, the patient was taken into routine follow-up (Figure 6).

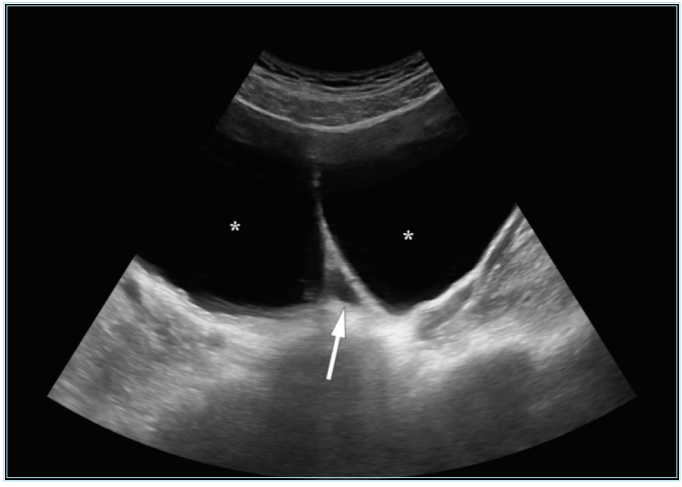

Figure 1. Ultrasonography image demonstrating a large volume bladder with a double lumen appearance (stars) and a dilated left ureter (arrow)

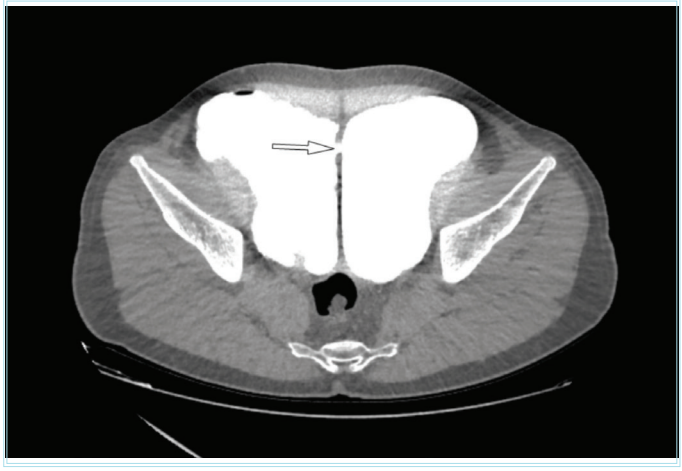

Figure 2. Computed tomography image demonstrating the narrow neck (arrow) between the bladder lumen on the right and the diverticulum on the left

Discussion

Bladder diverticula are divided into two groups: congenital and acquired.[4] It can also be iatrogenic.[5] Congenital and acquired bladder diverticula are more common in men.[6] Congenital bladder diverticulum is thought to be due to a congenital weakness in the bladder wall musculature, and there is usually a single diverticulum.[7] Acquired diverticula are usually multiple. The most common cause of acquired diverticula is thought to result from increased intravesical pressure.[8] The most common etiologies of increased intravesical pressure

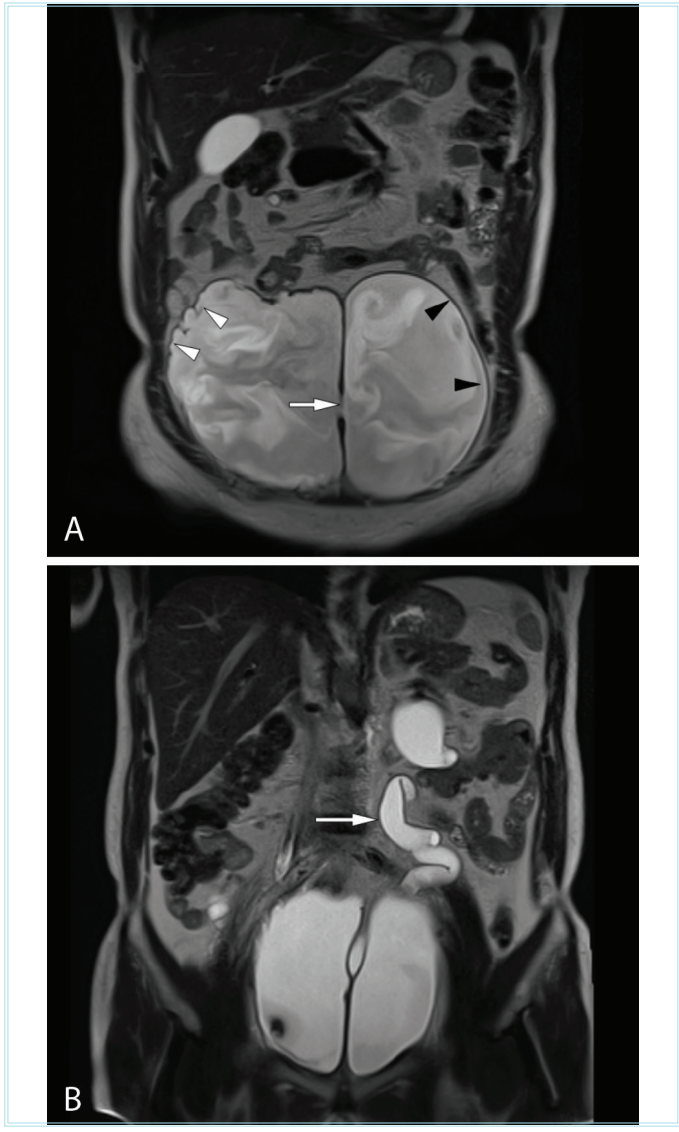

Figure 3. Magnetic resonance imaging (MRI) demonstrating narrow neck (arrow) between the diverticulum and the bladder lumen, trabeculated appearance on the bladder wall (white arrowheads), a thin wall structure of diverticulum (black arrowheads) (A). MRI demonstrating the left ureter between the diverticulum and the bladder, dilated and tortuous proximal to this level (arrow) (B)

include benign prostatic hyperplasia, urethral stricture and voiding dysfunction.[1] Bladder diverticulum is usually asymptomatic and diagnosed incidentally. In those who are symptomatic, the symptoms are often atypical, leading to a delay in diagnosis.[3] The most common presentation is recurrent urinary tract infection secondary to residue in the diverticulum. Other reported presentations include acute urinary retention, bladder stones, enuresis, voiding dysfunction, and bladder obstruction.[9] Our patient presented with bilateral inguinal pain, dysuria, and a palpable mass in the abdomen.

US, CT, MRI, and VCUG can be used to diagnose diverticula. We used all of these imaging methods when diagnosing the condition.

The surgical methods include open or laparoscopic diverticulectomy.[10] We preferred open diverticulectomy in our patient. Diverticulectomy can be performed by an extravesical, intravesical, or combined approach with good results. The basic principle is to dissect close to the wall of the diverticulum, while the bladder muscle defect must be meticulously repaired.[7] We operated on our patient using an extravesical approach. There were no complications after surgery, and the patient was discharged.

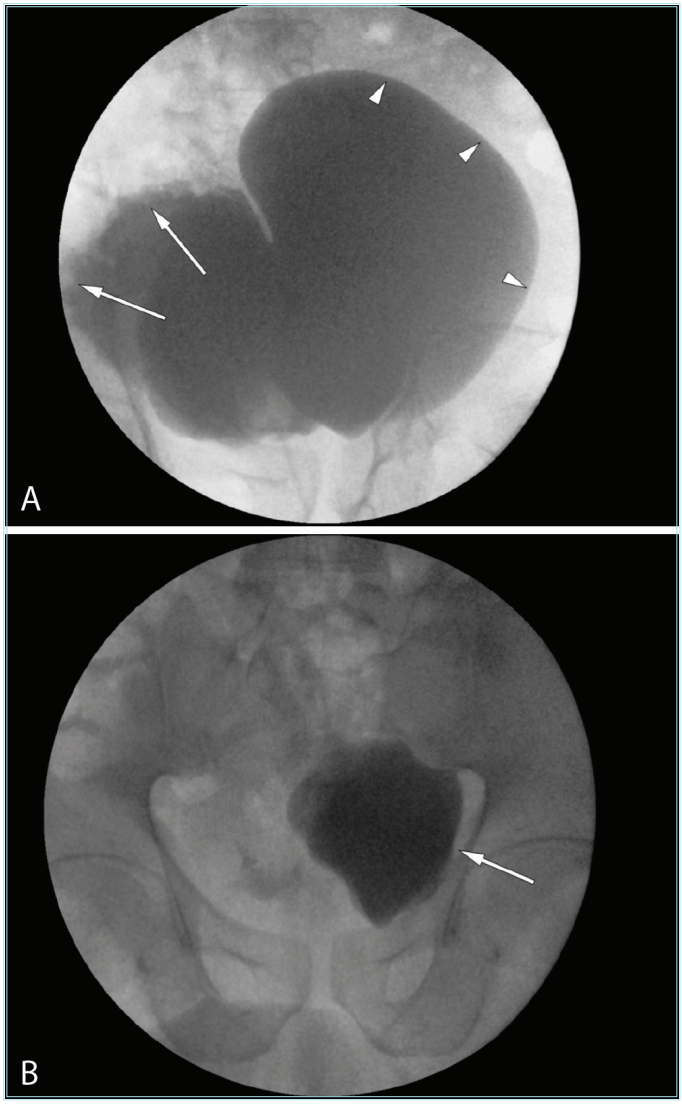

Figure 4. VCUG image demonstrating increased bladder trabeculation (arrows), a giant diverticulum with smooth borders (arrowheads) (A). The image taken after re-catheterization demonstrating completely emptied bladder and significant residue remained in the diverticulum (arrow) (B)

VCUG: Voiding cystourethrography

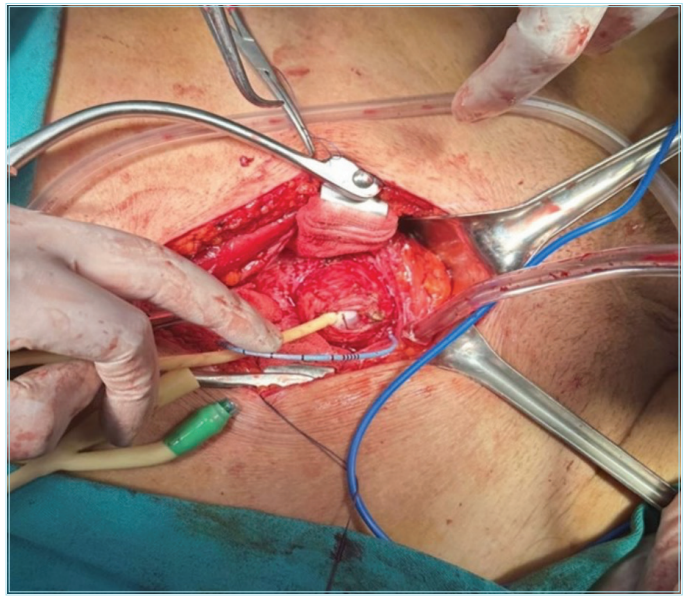

Figure 5. Location of the diverticulum neck

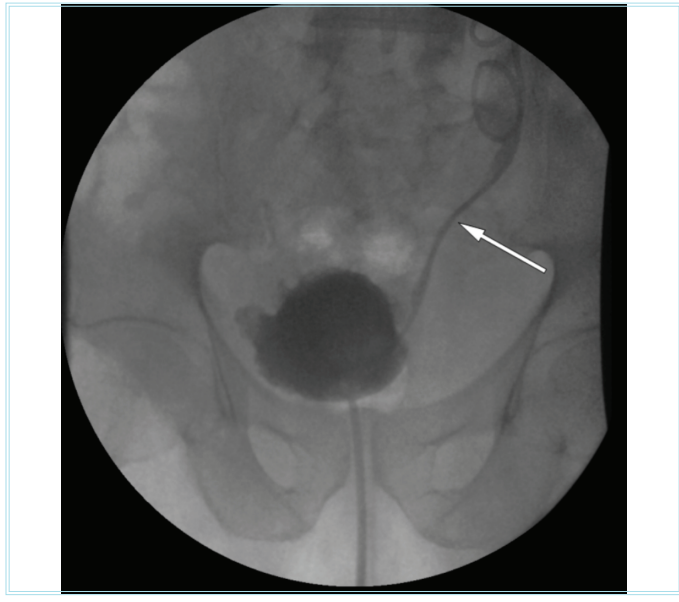

Figure 6. Retrograde cystography demonstrating no leakage outside the bladder. Double J catheter is seen on the left (arrow)

Conclusion

Bladder megadiverticula may be asymptomatic or their findings may be confused with many diseases. Therefore, making the correct diagnosis is crucial in treatment.

Ethics

Informed Consent: Consent form was filled out by all participants.

Footnotes

Authorship Contributions

Surgical and Medical Practices: Ç.K., Ö.Ç., S.B., Concept: K.N.A., Design: T.Ç., Data Collection or Processing: K.N.A., T.Ç., Analysis or Interpretation: K.N.A., T.Ç., Literature Search: K.N.A., T.Ç., Writing: K.N.A., T.Ç., Ç.K., Ö.Ç.

Conflict of Interest: No conflict of interest was declared by the authors.

Financial Disclosure: The authors declared that this study received no financial support.

References

1. Kumar S, Jayant K, Barapatra Y, Rani J, Agrawal S. Giant urinary bladder diverticula presenting as epigastric mass and dyspepsia. Nephrourol Mon. 2014;6:e18918.
2. Appeadu-Mensah W, Hesse AA, Yaw MB. Giant bladder diverticulum: a rare cause of bladder outlet obstruction in children. Afr J Paediatr Surg. 2012;9:83-7.
3. Sow O, Sarr A, Ze Ondo C, Sine B, Ndiath A, Ndoye AK. Giant bladder diverticulum in a postmenopausal woman: case report and literature review. Urol Case Rep. 2021;39:101807.
4. Senel S, Kizilkan Y, Bulut S, Aktas BK. (2020). Giant bladder diverticulum: A case report and review of the literature. Ann Clin Anal Med. 2020:1-4.
5. Chia-Yu Chang J, Hsu TF, How CK. Acute urine retention with two giant urinary bladder diverticula. J Emerg Med. 2015;48:e39-40.
6. Levard G, Aigrain Y, Ferkadji L, Elghoneimi A, Pichon J, Boureau M. Urinary bladder diverticula and the Ehlers-Danlos syndrome in children. J Pediatr Surg. 1989;24:1184-6.
7. Sheldon CA, Essig KA. Congenital bladder diverticulum causing bladder outlet obstruction: case report and review of the literature. Pediatr Surg Int. 1994;9:141-3.
8. Silberman M, Jeanmonod R. Bladder diverticulitis: a case report. Case Rep Emerg Med. 2011;2011:303498.
9. Jiang S, Ren Q, Wang X, et al. A huge bladder diverticulum in an elderly: A case report. SAGE Open Med Case Rep. 2020;8:2050313X20943475.
10. Vaddi S, Pogula V, Devraj R, Sreedhar A. Congenital bladder diverticulum - a rare adult presentation. J Surg Case Rep. 2011;2011:8.